Electronic Supplementary Information for

Probing twisted intramolecular charge transfer of pyrene derivatives as organic emitters in OLEDs

Young Mo Sung,[a] Eun Suk Kwon,[b] Yusuke Makida Maruyama,[b] Youngsik Shin,[a] Soo-Ghang Ihn,[b] Jong Soo Kim,[b] Hyeonho Choi,[b] Hyo Sug Lee,[a] Jung-Hwa Kim,[a] Joonghyuk Kim,[b] Soohwan Sul[a]**

[a]Analytical Engineering Group, Samsung Advanced Institute of Technology, 130, Samsung-ro, Yeongtong-gu, Suwon-si, Gyeonggi-do, 16678, South Korea

[b]Organic Materials Lab, Samsung Advanced Institute of Technology, 130, Samsung-ro, Yeongtong-gu, Suwon-si, Gyeonggi-do, 16678, South Korea

Table of Contents

1. Experimental Details

Synthesis of the pyrene derivatives

Pyr1. [Step 1] 4-Bromobiphenyl (8.71 g, 37.4 mmol, 1.2 equiv.), bis(dibenzylideneacetone)palladium (1.73 g, 3.0 mmol, 10%), and sodium *tert*-butoxide (5.84 g, 60.8 mmol, 2.0 equiv.) were placed in a 250-mL three-necked flask. The flask was evacuated and backfilled with N_2 (3×), after which toluene (80 mL), 3-aminobiphenyl (4.90 mL, 31.3 mmol, 1.0 equiv.), and tri-*tert*-butylphosphine (50 wt% in toluene, 1.3 mL, 3.1 mmol, 10%) were added, and the resulting mixture was stirred at 110 °C for 10 h. After cooling to ~60 °C, the reaction mixture was filtered through a pad of silica gel. The filtrate was concentrated and the residue was separated by flash column chromatography on silica gel (hexane/dichloromethane 15–40%) to furnish *N*-([1,1′-biphenyl]-4-yl)-[1,1′-biphenyl]-3-amine (**Pyr1-P2**) as a white solid (2.95 g, 9.2 mmol, 97.7% pure by LCMS). **LRMS-APCI** (*m*/*z*): $[M+H]^+$ calcd. for $[C_{24}H_{20}N]^+$ 322.16; found 322.15.

[Step 2] A 500 mL three-necked-flask was charged with 9*H*-carbazole (3.76 g, 22.4 mmol, 1.0 equiv.), 1,6-dibromopyrene (12.12 g, 33.6 mmol, 1.5 equiv.), bis(dibenzylidenacetone)palladium (0.34 g, 0.56 mmol, 2.5%), Xantphos (0.39 g, 0.67 mmol, 3.0%), and sodium *tert*-butoxide (4.27 g, 44.8 mmol, 2.0 equiv.). The flask was evacuated and backfilled with N_2 (3×), after which toluene (225 mL) was added. The resulting mixture was stirred at 110 °C for 22 h. After cooling to rt, the reaction mixture was filtered through a pad of silica gel. The filtrate was concentrated and the residue was separated by flash column

chromatography on silica gel (hexane/dichloromethane 5–25%) to furnish 9-(6-bromopyren-6-yl)-9*H*-carbazole (**Pyr1-P1**) as a white solid (4.76g, 9.2 mmol, 99.1% pure by LCMS). **LRMS-APCI** (*m*/*z*): $[M]^+$ calcd. for $[C_{28}H_{16}NBr]^+$ 445.05, 447.05; found 445.04, 447.04. [Step3] **Pyr1-P1** (1.29 g, 2.9 mmol, 1.0 equiv.), **Pyr1-P2** (0.97 g, 3.1 mmol, 1.1 equiv.), bis(dibenzylidenacetone)palladium (0.16 g, 0.28 mmol, 10%), and sodium *tert*-butoxide (0.55 g, 5.8 mmol, 2.0 equiv.) were placed in a 250-mL three-necked flask. The flask was evacuated and backfilled with N_2 (3×), after which toluene (65 mL) and tri-*tert*-butylphosphine (50 wt% in toluene, 0.12 mL, 0.30 mmol, 10%) were added, and the resulting mixture was stirred at 110 °C for 8 h. After cooling to ~60 °C, the reaction mixture was filtered through a pad of silica gel. The filtrate was concentrated and the residue was separated by flash column chromatography on silica gel (hexane/ethyl acetate 5–40%) to afford *N*-([1,1′-biphenyl]-3-yl)-*N*-([1,1′-biphenyl]-4-yl)-6-(9*H*-carbazol-9-yl)pyrene-1-amine (**Pyr1**) as a yellow solid (1.51 g, 2.2 mmol, 99.8% pure by LCMS). **^{1}H NMR** (400 MHz, CD_2Cl_2) δ 8.37 (d, 1H, J = 5.5 Hz), 8.34 (d, 1H, J = 4.8 Hz), 8.30–8.26 (m, 2H), 8.24 (d, 1H, J = 4.9 Hz), 8.12 (dd, 2H, J = 5.2, 4.3 Hz), 7.79 (dd, 2H, J = 5.2, 4.4 Hz), 7.59 (dd, 2H, J = 5.0, 0.8 Hz), 7.55–7.46 (m, 5H), 7.46–7.39 (m, 3H), 7.39–7.24 (m, 10H), 7.23–7.17 (d, 2H, J = 8.5 Hz), 7.10 (ddd, 1H, J = 4.8, 1.4, 0.6 Hz), 7.03 (dd, 2H, J = 4.1, 1.0 Hz); **^{13}C{^{1}H} NMR** (125 MHz, CD_2Cl_2) δ 149.6, 148.6, 143.0, 142.9, 142.1, 141.4, 141.0, 135.1, 132.0, 131.8, 130.3, 130.1, 129.4, 129.3, 129.2, 129.0, 128.9, 128.8, 128.33, 128.26, 128.0, 127.6, 127.53, 127.46, 127.37, 127.0, 126.9, 126.6, 126.5, 126.4, 124.7, 123.9, 122.9, 122.8, 121.9, 121.61, 121.57, 120.9, 120.5, 110.7; **LRMS-APCI** (*m*/*z*): $[M+H]^+$ calcd. for $[C_{52}H_{35}N_2]^+$ 687.28; found 687.27.

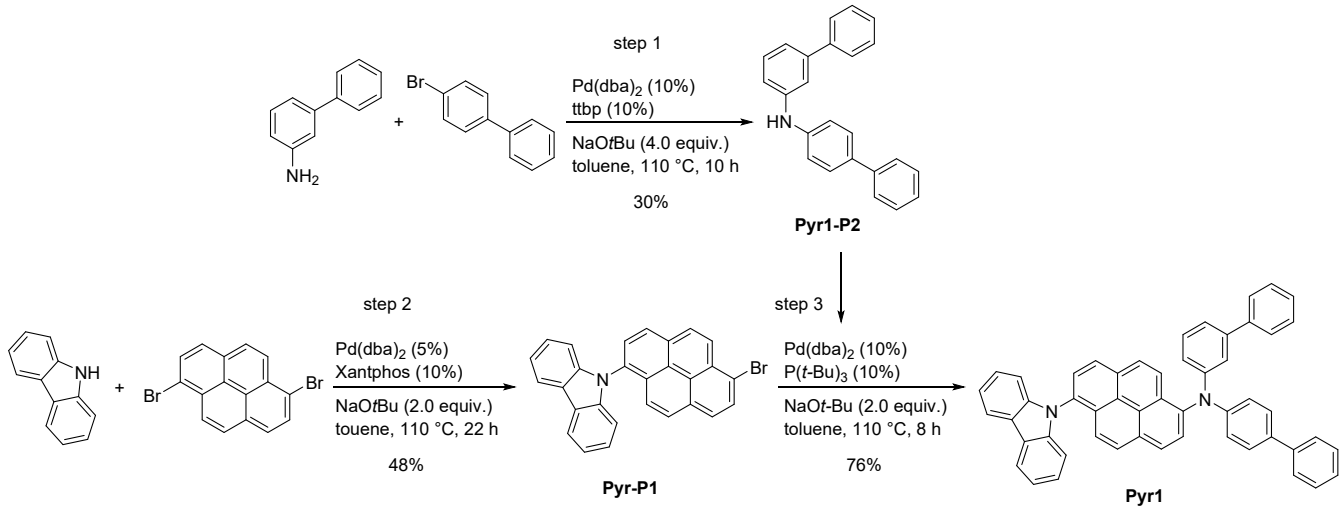

Figure S1. Procedure for the synthesis of **Pyr1**.

Pyr3. [Step 1] 2-Aminobiphenyl (4.83 g, 28.5 mmol, 1.0 equiv.), 4-bromobiphenyl (8.71 g, 37.4 mmol, 1.3 equiv.), bis(dibenzylidenacetone)palladium (1.73 g, 3.0 mmol, 10%), and sodium *tert*-butoxide (5.95 g, 61.9 mmol, 2.2 equiv.) were placed in a 250-mL three-necked flask. The flask was evacuated and backfilled with N_2 (3×), after which toluene (80 mL) and tri-*tert*-butylphosphine (50 wt% in toluene, 1.3 mL, 3.1 mmol, 10%) were added, and the resulting mixture was stirred at 110 °C for 20 h. After cooling to ~60 °C, the reaction mixture was filtered through a pad of silica gel. The filtrate was concentrated and the residue was separate by flash column chromatography on silica gel (hexane/dichloromethane 15–40%), which gave a 55:45 mixture of *N*-([1,1′-biphenyl]-4-yl)-[1,1′-biphenyl]-2-amine (**Pyr3-P2**) and the corresponding triarylamine (**A**) as a white solid (8.87 g, 92.8% pure as the sum of **Pyr3-P2** and **A** by LCMS). **LRMS-APCI** (*m*/*z*): $[M+H]^+$ calcd. for $[C_{24}H_{20}N]^+$ 322.16; found 322.16. The mixture was used in step 3 without further purification. [Step 2] See step 2 in the synthesis of **Pyr1** for details. [Step3] **Pyr1-P1** (1.38 g, 3.1 mmol, 1.0 equiv.), **Pyr3-P2** (~56% pure, 2.27 g, 3.2

mmol, 1.1 equiv.), bis(dibenzylideneacetone)palladium (0.17 g, 0.30 mmol, 10%), and sodium *tert*-butoxide (0.58 g, 6.0 mmol, 2.0 equiv.) were placed in a 250-mL three-necked flask. The flask was evacuated and backfilled with N_2 (3×), after which toluene (65 mL) and tri-*tert*-butylphosphine (50 wt% in toluene, 0.12 mL, 0.30 mmol, 10%) were added, and the resulting mixture was stirred at 110 °C for 10 h. After cooling to ~60 °C, the reaction mixture was filtered through a pad of silica gel. The filtrate was concentrated and the residue was separated by flash column chromatography on silica gel (hexane/ethyl acetate 5–40%) to afford *N*-([1,1′-biphenyl]-2-yl)-*N*-([1,1′-biphenyl]-4-yl)-6-(9*H*-carbazol-9-yl)pyrene-1-amine (**Pyr3**) as a yellow solid (1.60g, 2.3 mmol, 98.8% pure by LCMS). **^{1}H NMR** (400 MHz, CD_2Cl_2) δ 8.26 (dd, 2H, J = 4.0, 1.0 Hz), 8.22 (d, 1H, J = 4.8 Hz), 8.03 (d, 1H, J = 4.8 Hz), 7.97 (d, 1H, J = 5.0 Hz), 7.94 (d, 1H, J = 5.6 Hz), 7.83 (d, 1H, J = 5.6 Hz), 7.81 (d, 1H, J = 5.5 Hz), 7.58 (d, 1H, J = 4.9 Hz), 7.54 (d, 1H, J = 4.3 Hz), 7.52–7.24 (m, 16H), 7.20 (d, 2H, J = 4.1 Hz), 7.01 (d, 2H, J = 4.3 Hz), 6.91 (t, 2H, J = 4.6 Hz), 6.81 (t, 1H, J = 4.5 Hz); **^{13}C{^{1}H} NMR** (100 MHz, CD_2Cl_2) δ 150.1, 147.1, 143.0, 142.5, 141.1, 140.48, 140.43, 134.2, 132.7, 131.8, 131.2, 129.4, 129.32, 129.29, 129.2, 129.1, 128.9, 128.6, 128.2, 128.0, 127.3, 127.2, 126.95, 126.92, 126.7, 126.6, 126.37, 126.34, 126.33, 126.30, 126.0, 125.8, 125.7, 123.8, 121.8, 120.9, 120.4, 110.7 (two ^{13}C NMR signals are absent, which might be due to overlap with other signals.); **LRMS-APCI** (*m*/*z*): $[M+H]^+$ calcd. for $[C_{52}H_{35}N_2]^+$ 687.28; found 687.29.

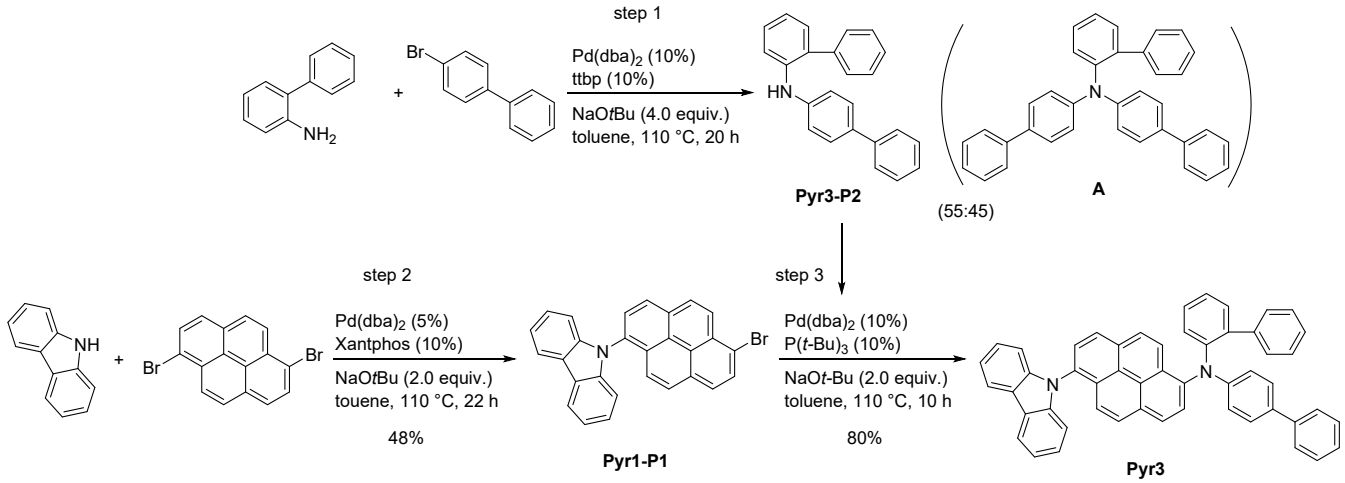

Figure S2. Procedure for the synthesis of **Pyr3**.

Pyr2. [Step 1] 3',5'-Di-*tert*-butyl-[1,1'-biphenyl]-3-amine (6.44 g, 22.9 mmol, 1.0 equiv.), 4'-bromo-3,5-di-*tert*-butyl-1,1'-biphenyl (8.70 g, 25.2 mmol, 1.1 equiv.), tris(dibenzylideneacetone)dipalladium (0.42 g, 0.5 mmol, 0.02 equiv.), sodium *tert*-butoxide (2.42 g, 25.2 mmol, 1.1 equiv.), tri-*tert*-butylphosphine (50 wt% in toluene, 0.19 g, 0.5 mmol, 0.02 equiv.), and xylene (115 mL) were placed in a 250-mL three-necked flask. The resulting mixture was stirred at 140 °C for 18 h. After cooling to room temperature, the reaction mixture was extracted with dichloromethane and water. The combined organic layers were dried over magnesium sulfate and evaporated with a rotary evaporator. The residue was separated by flash column chromatography on silica gel (hexane/dichloromethane 15–40%), which furnished 3',5'-di-tert-butyl-*N*-(3',5'-di-tert-butyl-[1,1'-biphenyl]-4-yl)-[1,1'-biphenyl]-3-amine (**Pyr2-P2**) as a white solid (8.60 g, 15.8 mmol, 97.4% pure by LCMS). **LRMS-APCI** (*m*/*z*): $[M+H]^+$ calcd. for $[C_{40}H_{52}N]^+$ 546.40; found 546.40. [Step 2] A 1-L three-necked flask was charged with 3,6-di-*tert*-butyl-9*H*-carbazole (15.01 g, 53.7 mmol, 1.0 equiv.), 1,6-dibromopyrene (23.21 g, 64.5 mmol, 1.2 equiv.), bis(dibenzylidenacetone)palladium (3.09 g, 5.4

mmol, 0.1 equiv.), Xantphos (6.22 g, 10.7 mmol, 0.2 equiv.), sodium *tert*-butoxide (15.48 g, 161.1 mmol, 3.0 equiv.) and toluene (890 mL). The resulting mixture was stirred at 95 °C for 24 h. After cooling to room temperature, the reaction mixture was filtered through a pad of silica gel with dichloromethane. The filtrate was concentrated and the residue was separated by flash column chromatography on silica gel (hexane/dichloromethane 10–20%), which furnished 9-(6-bromopyren-1-yl)-3,6-di-*tert*-butyl-9*H*-carbazole (**Pyr2-P1**) as a white solid (8.41g, 15.1 mmol, 99.3% pure by LCMS). **LRMS-APCI** (*m*/*z*): $[M]^+$ calcd. for $[C_{36}H_{33}NBr]^+$ 558.17; found 558.17. [Step3] A 50-mL three-necked flask was charged with **Pyr2-P1** (0.66 g, 1.2 mmol, 1.0 equiv.), **Pyr2-P2** (0.70 g, 1.3 mmol, 1.1 equiv.), bis(dibenzylidenacetone)palladium (0.07 g, 0.1 mmol, 0.1 equiv.), potassium *tert*-butoxide (0.40 g, 3.5 mmol, 3.0 equiv.), tri-*tert*-butylphosphine (50 wt% in toluene, 0.10 g, 0.2 mmol, 0.2 equiv.), and toluene (5 mL). The resulting mixture was stirred at 95 °C for 2 h. After cooling to room temperature, the reaction mixture was diluted with methanol and filtered. The resulting solid was dissolved in toluene and filtered through a pad of silica gel. The filtrate was concentrated and recrystallized from toluene to give 6-(3,6-di-*tert*-butyl-9*H*-carbazol-9-yl)-*N*-(3',5'-di-*tert*-butyl-[1,1'-biphenyl]-3-yl)-*N*-(3',5'-di-*tert*-butyl-[1,1'-biphenyl]-4-yl)pyrene-1-amine (**Pyr2**) as a yellow solid (0.63g, 0.6 mmol, 99.9% pure by LCMS). **^{1}H NMR** (500 MHz, C_2Cl_6) δ 8.37 (d, J = 9.3 Hz, 1H), 8.32 (d, J = 8.2 Hz, 1H), 8.28 (d, J = 1.8 Hz, 2H), 8.24 (d, J = 8.2 Hz, 1H), 8.13 (d, J = 9.3 Hz, 1H), 8.07 (d, J = 8.0 Hz, 1H), 7.98 (d, J = 8.0 Hz, 1H), 7.97 (d, J = 9.3 Hz, 1H), 7.50 (d, J = 9.2 Hz, 1H), 7.51 (d, J = 8.6 Hz, 2H), 7.42 (dd, J = 8.4, 1.9 Hz, 2 H), 7.40 (s and d overlap, 3H), 7.36 (t, J = 1.7 Hz, 1H), 7.33 (t, J = 1.9 Hz, 1H), 7.31 (t, J = 7.9 Hz, 1H), 7.25 (d, J = 8.6 Hz, 2H), 7.25 (d, J = 1.7 Hz, 2H), 7.21 (d, J = 7.7 Hz, 1H), 7.06 (dd, J = 8.0, 2.1 Hz, 1H), 6.95 (d, J = 8.1 Hz, 2H), 1.48 (s, 18 H), 1.36

(s, 18H), 1.27 (s, 18H). **$^{13}C\{^{1}H\}$ NMR** (126 MHz, C_2Cl_2) δ 151.8, 151.7, 149.4, 148.3, 144.2, 143.5, 142.1, 141.5, 141.0, 140.6, 136.7, 132.3, 131.7, 130.1, 130.0, 129.3, 128.8, 128.7, 128.69, 127.5, 127.3, 1263, 124.7, 124.3, 123.8, 123.2, 122.9, 122.2, 122.1, 121.7, 121.6, 121.5, 121.1, 117.0, 110.1, 35.4, 35.3, 35.3, 32.4, 31.8, 31.7. **LRMS-APCI** (*m*/*z*): $[M]^+$ calcd. for $[C_{76}H_{83}N_2]^+$ 1023.65; found 1023.68.

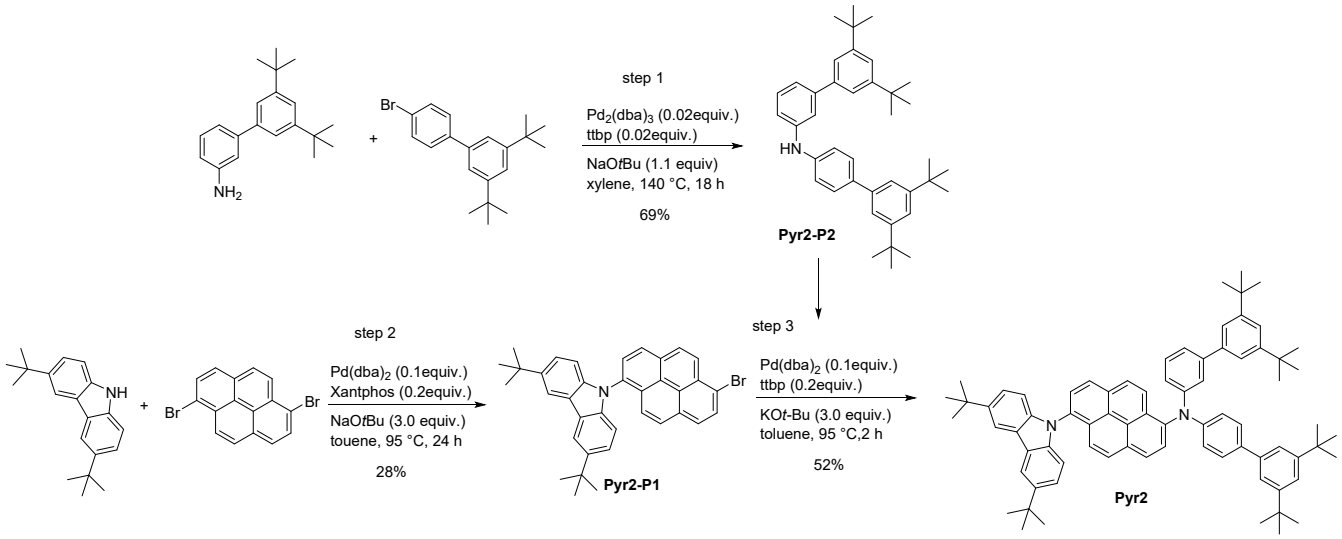

Figure S3. Procedure for the synthesis of **Pyr2**.

Pyr4. [Step 1] 3',5'-Di-*tert*-butyl-[1,1'-biphenyl]-2-amine (5.67 g, 20.2 mmol, 1.0 equiv.), 4'-bromo-3,5-di-tert-butyl-1,1'-biphenyl (7.66 g, 22.2 mmol, 1.1 equiv.), tris(dibenzylideneacetone)dipalladium (0.37 g, 0.4 mmol, 0.02 equiv.), sodium *tert*-butoxide (2.13 g, 22.2 mmol, 1.1 equiv.), tri-*tert*-butylphosphine (50 wt% in toluene, 0.16 g, 0.4 mmol, 0.02 equiv.) and xylene (101 mL) were placed in a 250-mL three-necked flask. The resulting mixture was stirred at 140 °C for 18 h. After cooling to room temperature, the reaction mixture was extracted with dichloromethane and water. The combined organic layers were dried over magnesium sulfate and evaporated with a rotary evaporator. The residue was separated by flash column chromatography on silica gel (hexane/dichloromethane 15–40%), which furnished 3',5'-di-*tert*-butyl-*N*-(3',5'-di-tert-butyl-[1,1'-biphenyl]-4-yl)-[1,1'-biphenyl]-2-amine

(**Pyr4-P2**) as a white solid (4.90 g, 9.0 mmol, 99.7% pure by LCMS). **LRMS-APCI** (*m*/*z*): $[M+H]^+$ calcd. for $[C_{40}H_{52}N]^+$ 546.40; found 546.40. [Step 2] See step 2 in the synthesis of **Pyr2** for details. [Step3] A 50-mL three-necked-flask was charged with **Pyr2-P1** (1.80 g, 3.2 mmol, 1.0 equiv.), **Pyr4-P2** (1.94 g, 3.6 mmol, 1.1 equiv.), bis(dibenzylidenacetone)palladium (0.19 g, 0.3 mmol, 0.1 equiv.), potassium *tert*-butoxide (1.09 g, 9.7 mmol, 3.0 equiv.), tri-*tert*-butylphosphine (50 wt% in toluene, 0.26 g, 0.6 mmol, 0.2 equiv.) and toluene (8 mL). The resulting mixture was stirred at 95 °C for 2 h. After cooling to room temperature, the reaction mixture was diluted with methanol and filtered. The resulting solid was separated by flash column chromatography on silica gel (hexane/dichloromethane 2–20%) to afford 6-(3,6-di-*tert*-butyl-9*H*-carbazol-9-yl)-*N*-(3',5'-di-*tert*-butyl-[1,1'-biphenyl]-2-yl)-*N*-(3',5'-di-tert-butyl-[1,1'-biphenyl]-4-yl)pyrene-1-amine (**Pyr4**) as a yellow solid (1.50g, 1.5 mmol, 98.7% pure by LCMS). **^{1}H NMR** (500 MHz, CD_2Cl_2) δ 8.27 (d, J = 1.6 Hz, 2H), 8.18 (d, *J* = 8.1 Hz, 1H), 7.99 (d, *J* = 8.2 Hz, 1H), 7.98 (d, *J* = 7.9 Hz, 1H), 7.83 (dd, *J* = 9.3, 3.1 Hz, 2H), 7.77 (d, *J* = 9.3 Hz, 1H), 7.61 (d, *J* = 8.2 Hz, 1H), 7.48 (dd, *J* = 8.2, 1.1 Hz, 1H), 7.25~7.44 (overlapped m, 11H), 6.80~7.1 (overlapped m, 7H), 1.48(s, 18H), 1.35 (s, 18H), 0.94 (s, 18H). **^{13}C{^{1}H} NMR** (126 MHz, CD_2Cl_2) *δ* 150.7, 149.3, 148.8, 146.5, 142.4, 141.8, 140.8, 140.6, 139.7, 139.0, 134.4, 131.8, 130.7, 130.5, 128.4, 128.0, 127.8, 127.8, 127.5, 127.2, 126.2, 125.9, 125.8, 125.6, 125.4, 125.4, 124.6, 124.5, 124.1, 123.3, 122.8, 122.2, 121.1, 120.8, 120.6, 120.4, 116.0, 109.1, 34.4, 34.3, 33.9, 31.4, 30.9, 30.4. **LRMS-APCI** (*m*/*z*): $[M]^+$ calcd. for $[C_{76}H_{83}N_2]^+$ 1023.65; found 1023.63.

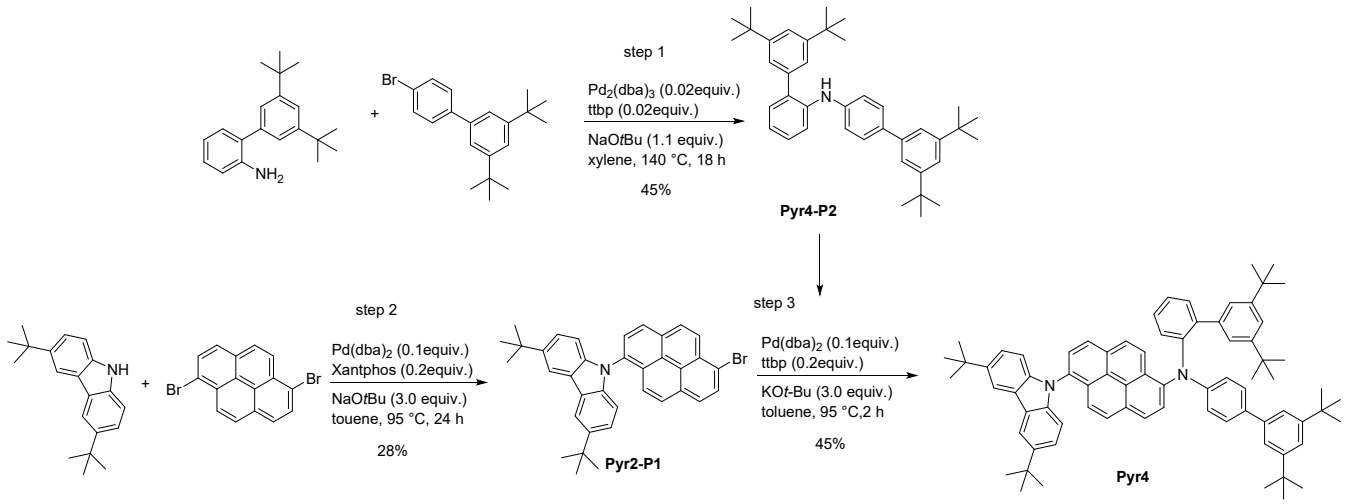

Figure S4. Procedure for the synthesis of **Pyr4**.

Steady-state absorption spectroscopy. UV/Vis/NIR absorption spectra were recorded using a commercial absorption spectrophotometer (Varian, Cary5000). A quartz cell (Hellma) with an optical path length of 10 mm was used for all steady-state experiments.

Photoluminescence spectroscopy

Photoluminescence spectra and lifetimes were recorded using a commercial fluorescence lifetime spectrometer (PicoQuant, Fluotime 300). A 379-nm diode laser and Xe lamp (PicoQuant) were used for photoexcitation.

Femtosecond transient absorption spectroscopy

An optical parametric amplifier (OPA; TOPAS, Light conversion) pumped by a Ti:sapphire regenerative amplifier system (Libra, Coherent) operating at a 1 kHz repetition rate and connected to an optical detection system (Helios, Ultrafast Systems) produced pumped pulses with a pulse width of ~70 fs and an average power of 70 μW at 350 nm. White light continuum

(WLC) probe pulses were generated using a 3-mm-thick sapphire window by focusing a small portion of the fundamental 800 nm pulses. The time delay between the pump and probe pulses was carefully controlled by ensuring that the pump beam traveled along a variable optical delay. The femtosecond transient absorption signal (ΔA) was obtained at a specific time by chopping pump pulses at 500 Hz, and probe spectra were recorded alternately with and without the pump pulse.

Computational Methods

Quantum mechanical calculations were performed by the Gaussian03 program suite.[S1] All calculations were carried out by the density functional theory (DFT) method with the Becke's three-parameter hybrid exchange functional and the Lee-Yang-Parr correlation functional (B3LYP),[S2] employing a basis set containing 6-31G(d) for all atoms.[S2] Geometry optimization in the ground states and excited states were performed by density functional theory and time-dependent (TD)-DFT method. Geometry optimization in the excited states were performed by To simulate the ground-state absorption spectra, we used TD-DFT calculations with the same functional and basis set.[S3]

References

S1. Gaussian 03, Revision C.02, Frisch, M. J.; Trucks, G. W.; Schlegel, H. B.; Scuseria, G. E.; Robb,M. A.; Cheeseman, J. R.; Zakrzewski, V. G.; Montgomery, J. A., Jr.; Stratmann, R. E.; Burant, J. C.; Dapprich, S.; Millam, J. M.; Daniels, A. D.; Kudin, K. N.; Strain, M. C.; Farkas, O.; Tomasi,J.; Barone, V.; Cossi, M.; Cammi, R.; Mennucci, B.; Pomelli, C.; Adamo, C.; Clifford, S.; Ochterski, J.; Petersson, G. A.; Ayala, P. Y.; Cui, Q.; Morokuma, K.; Malick, D. K.; Rabuck, A.D.; Raghavachari, K.; Foresman, J. B.; Cioslowski, J.; Ortiz, J. V.; Stefanov, B. B.; Liu, G.; Liashenko, A.; Piskorz, P.; Komaromi, I.; Gomperts, R.; Martin, R. L.; Fox, D. J.; Keith, T.; Al-Laham, M. A.; Peng, C. Y.; Nanayakkara, A.; Gonzalez, C.; Challacombe, M.; Gill, P. M. W.; Johnson, B. G.; Chen, W.; Wong, M. W.; Andres, J. L.; Head-Gordon, M.; Replogle, E. S.; Pople, J. A.; Gaussian, Inc., Wallingford CT, **2004**.

S2. (a) Becke, A. D. *J. Chem. Phys.* **1993**, *98*, 5648–5652. (b) Lee, C.; Yang, W.; Parr, R. G. *Phys. Rev. B* **1988**, *37*, 785–789.

S3. Bauernschmitt, R.; Ahlrichs, R. *Chem. Phys. Lett*. **1996**, *256*, 454–464.

3. Supporting figures (Figures S5–S35, Tables S1-S4).

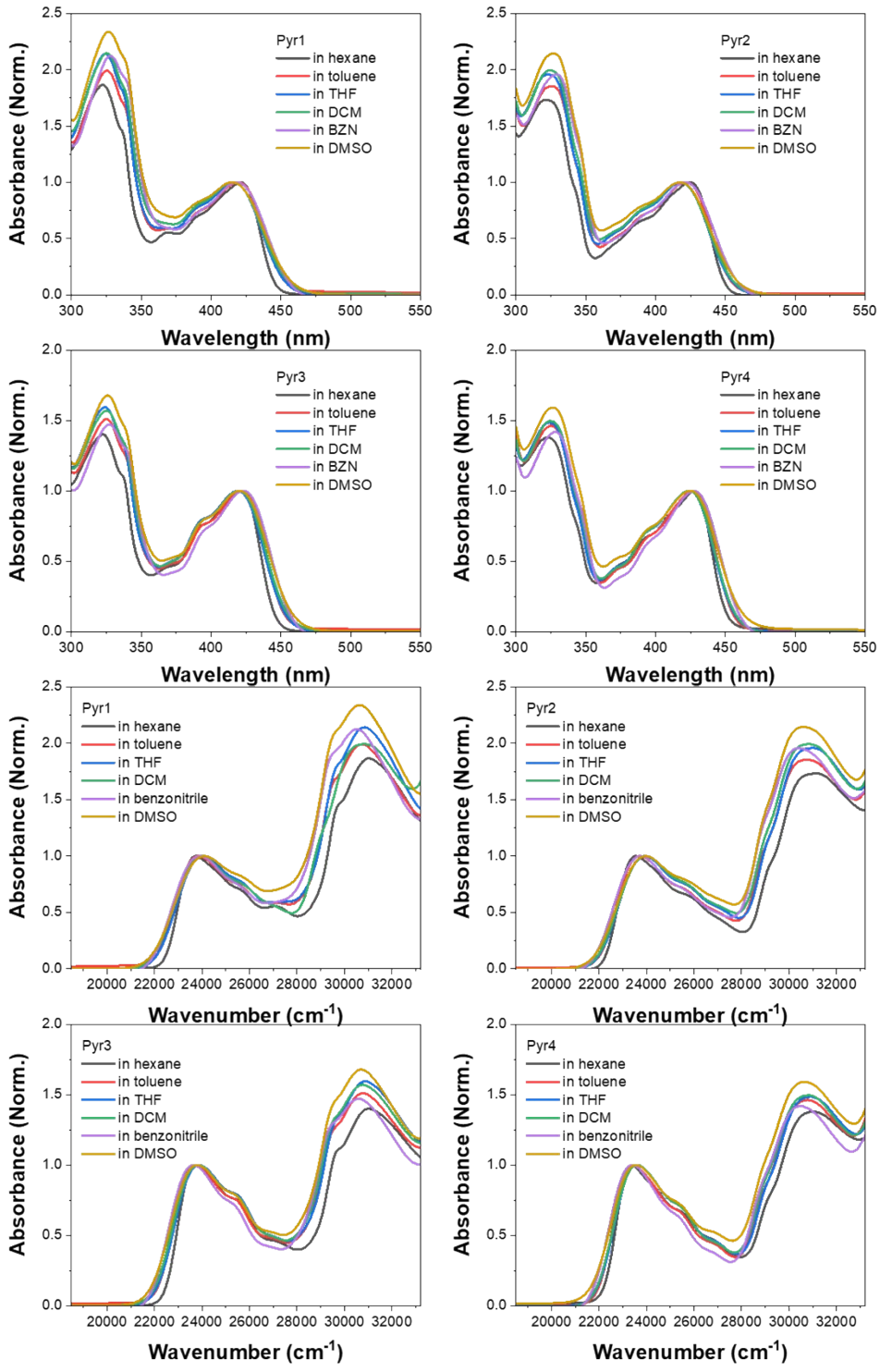

Figure S5. Normalized absorption spectra of the pyrene derivatives in this study in various solvents (hexane, toluene, THF, dichloromethane (DCM), benzonitrile (BZN), and DMSO).

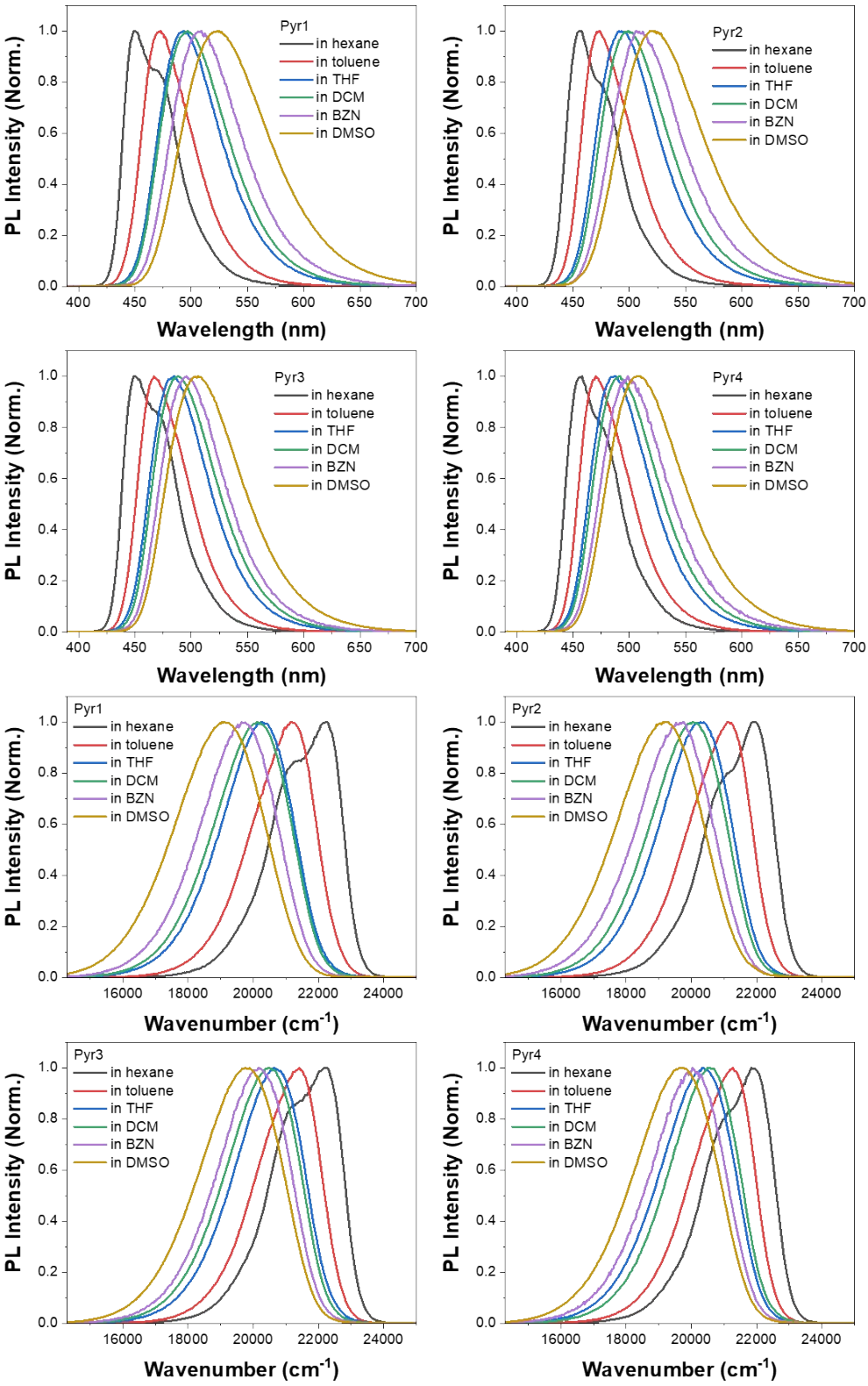

Figure S6. Normalized fluorescence spectra of the pyrene derivatives in this study in various solvents (hexane, toluene, THF, dichloromethane (DCM), benzonitrile (BZN), and DMSO)

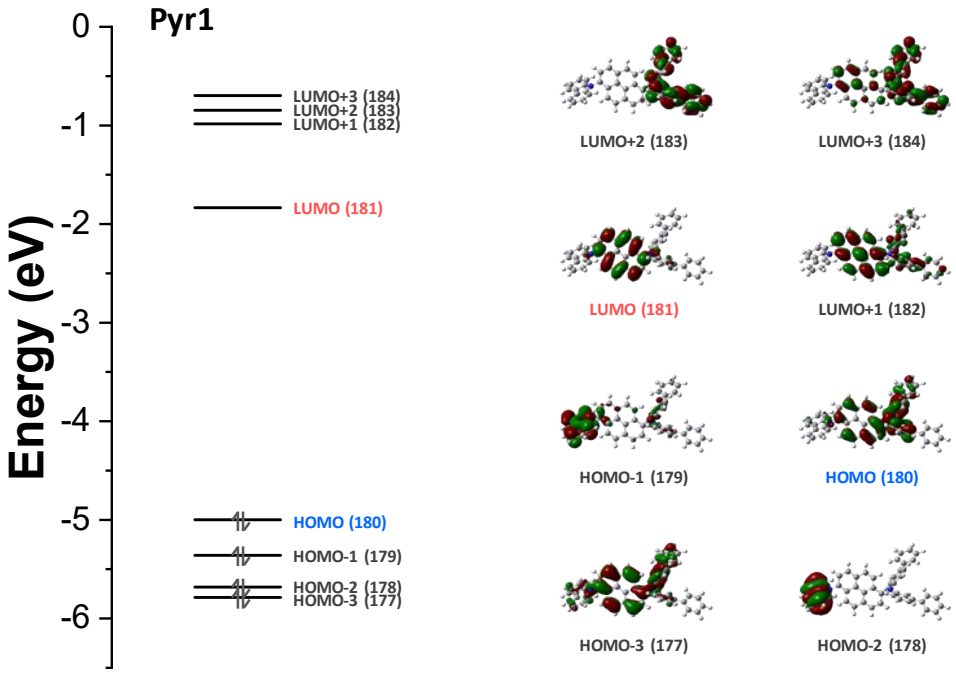

Figure S7. Energy-level diagram and molecular orbitals of **Pyr1**.

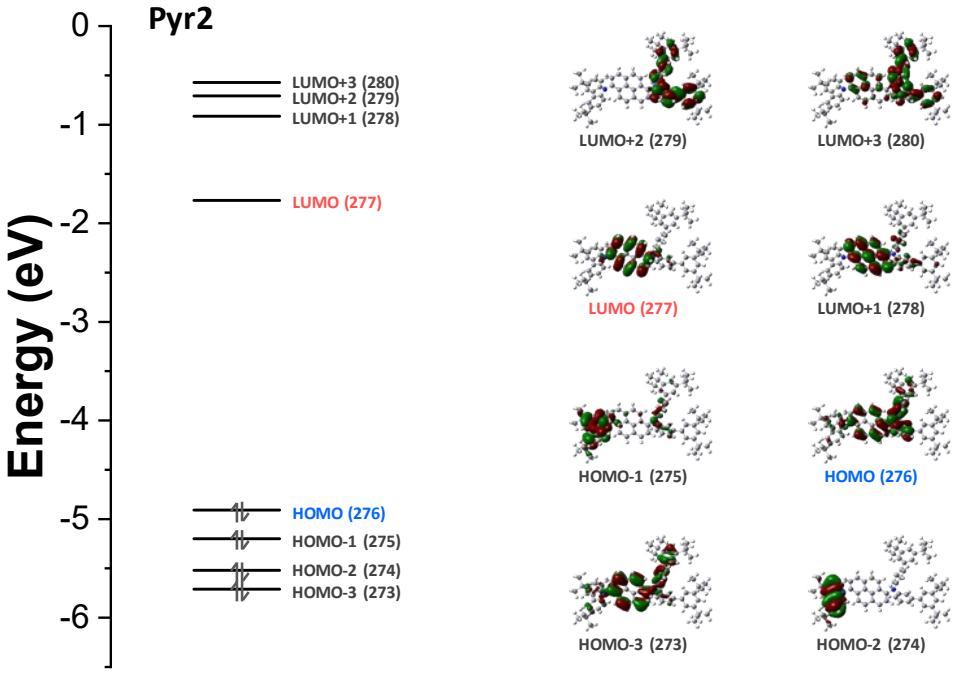

Figure S8. Energy-level diagram and molecular orbitals of **Pyr2**.

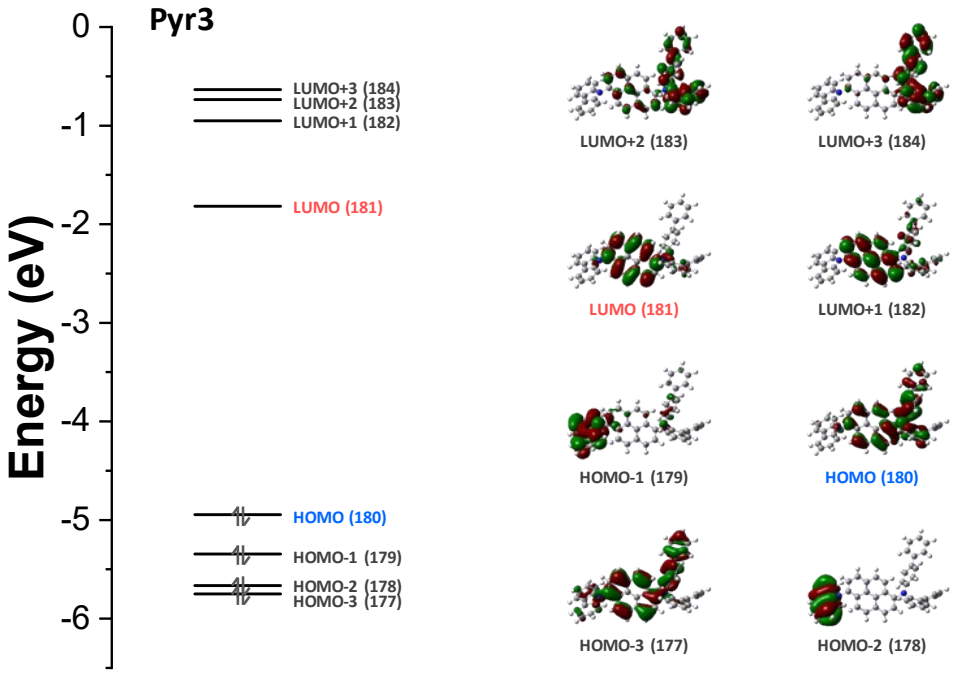

Figure S9. Energy-level diagram and molecular orbitals of **Pyr3**.

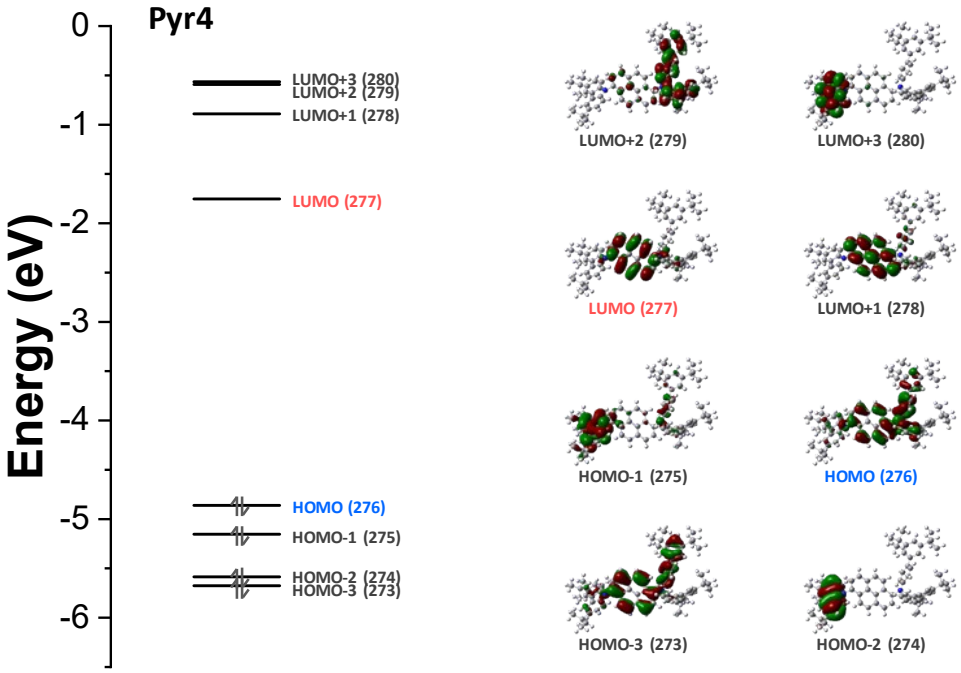

Figure S10. Energy-level diagram and molecular orbitals of **Pyr4**.

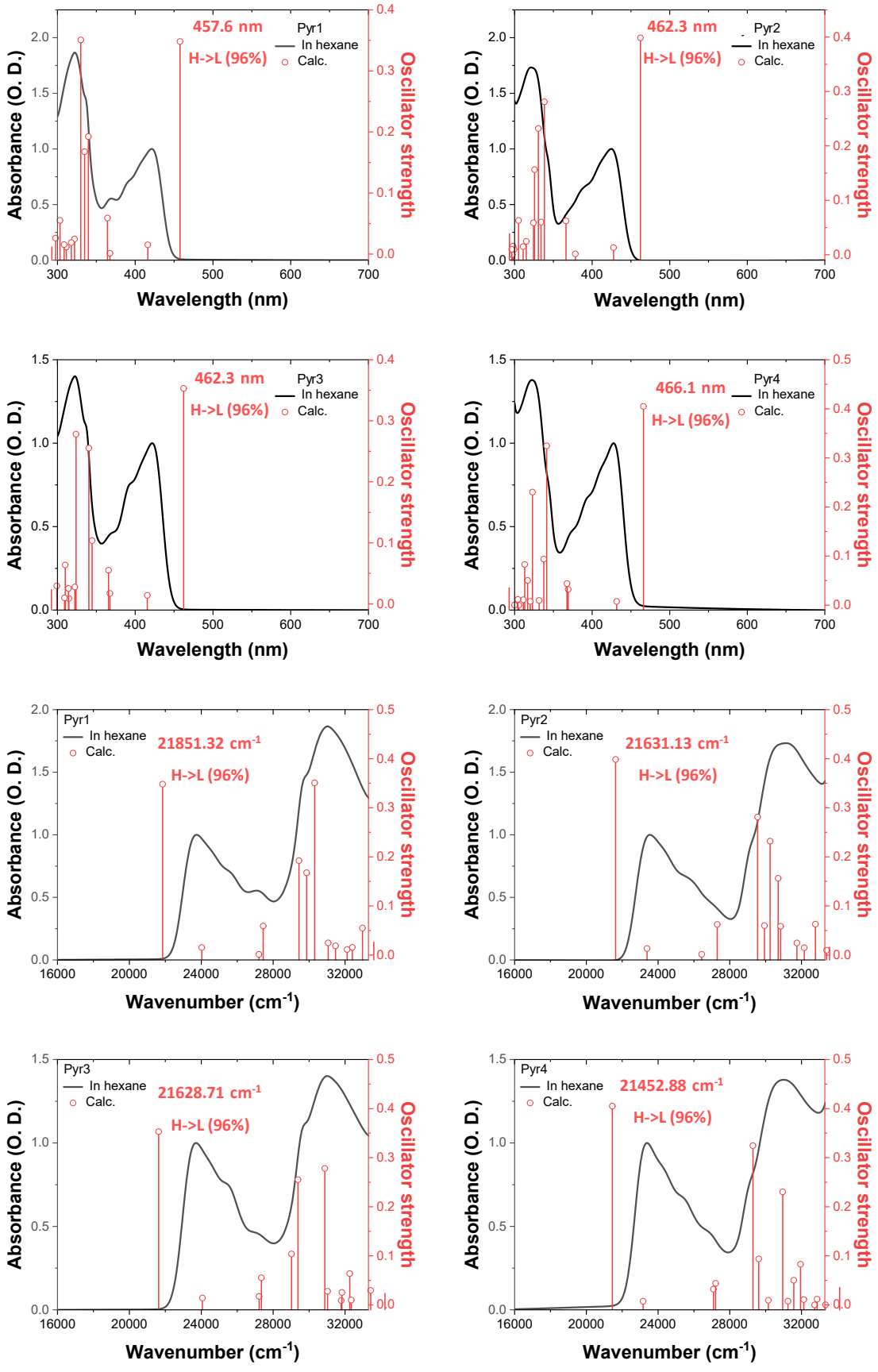

Figure S11. Absorption spectra and calculated vertical transitions for the pyrene derivatives in this study.

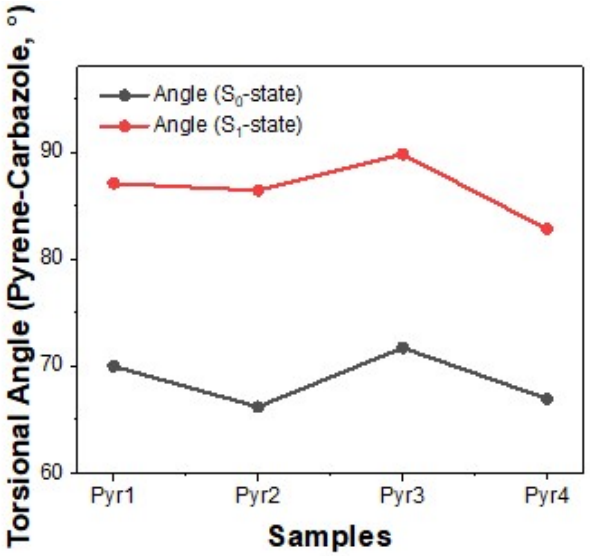

Figure S12. Torsional angles between the pyrene and carbazole substituent in the optimized S_0 and S_1 structures

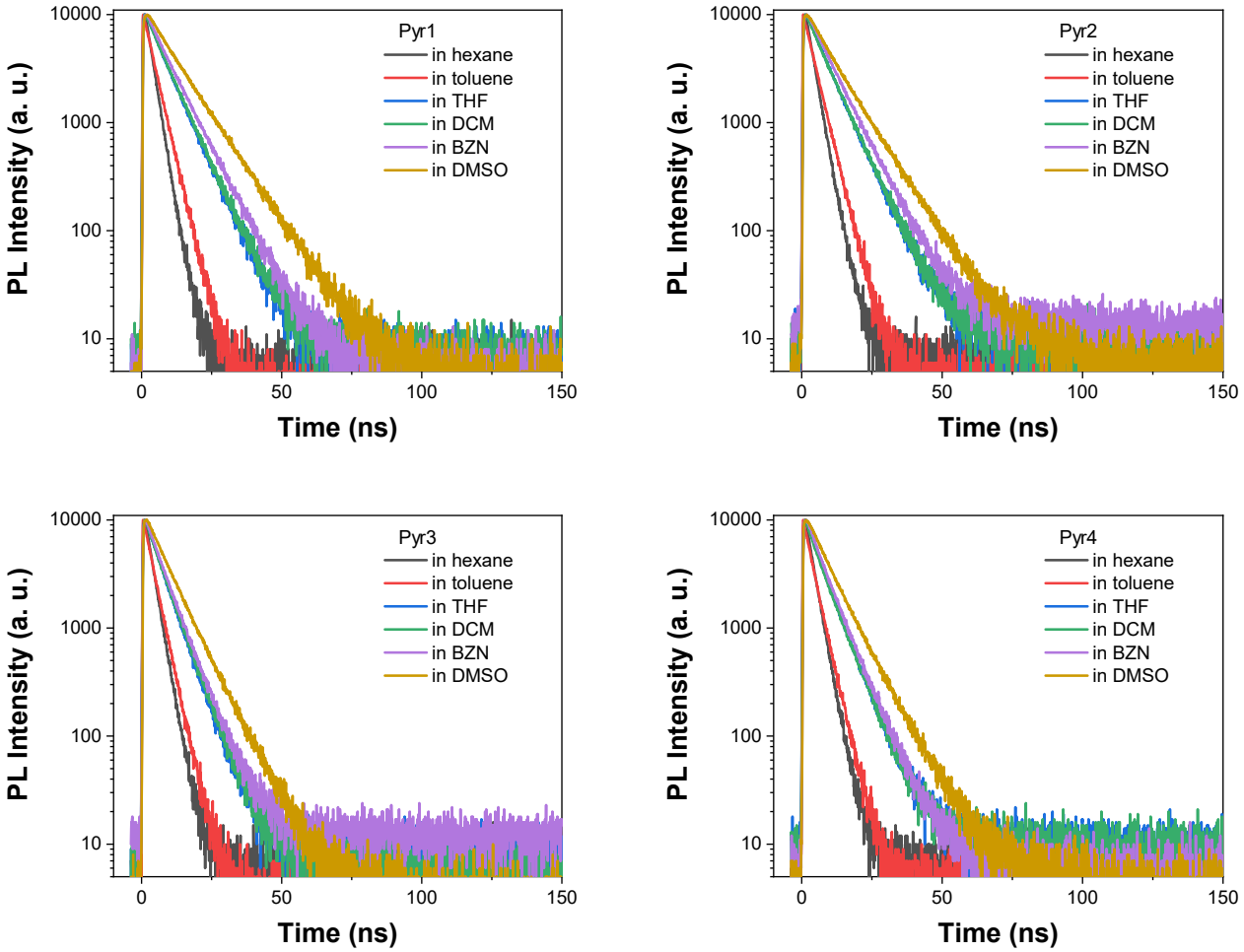

Figure S13. Time-resolved fluorescence decay profiles of the pyrene derivatives in this study in various solvents (hexane, toluene, THF, dichloromethane (DCM), benzonitrile (BZN), and DMSO).

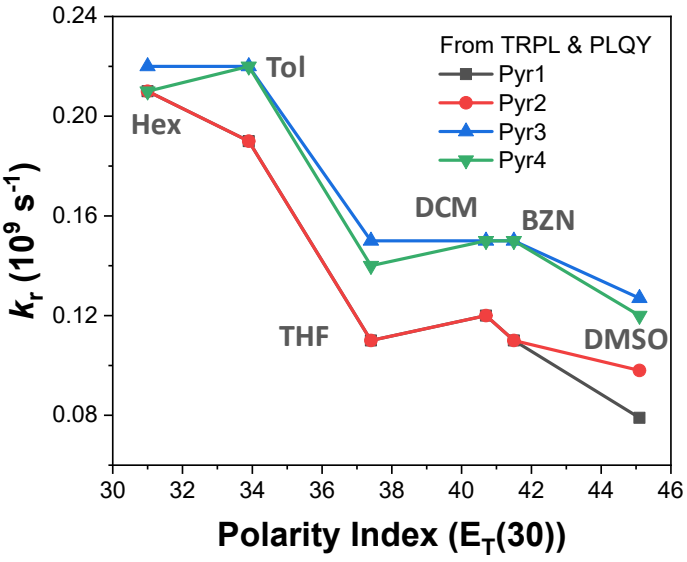

Figure S14. Radiative rates of the pyrene derivatives in various solvents (hexane, toluene, THF, dichloromethane (DCM), benzonitrile (BZN), and DMSO)

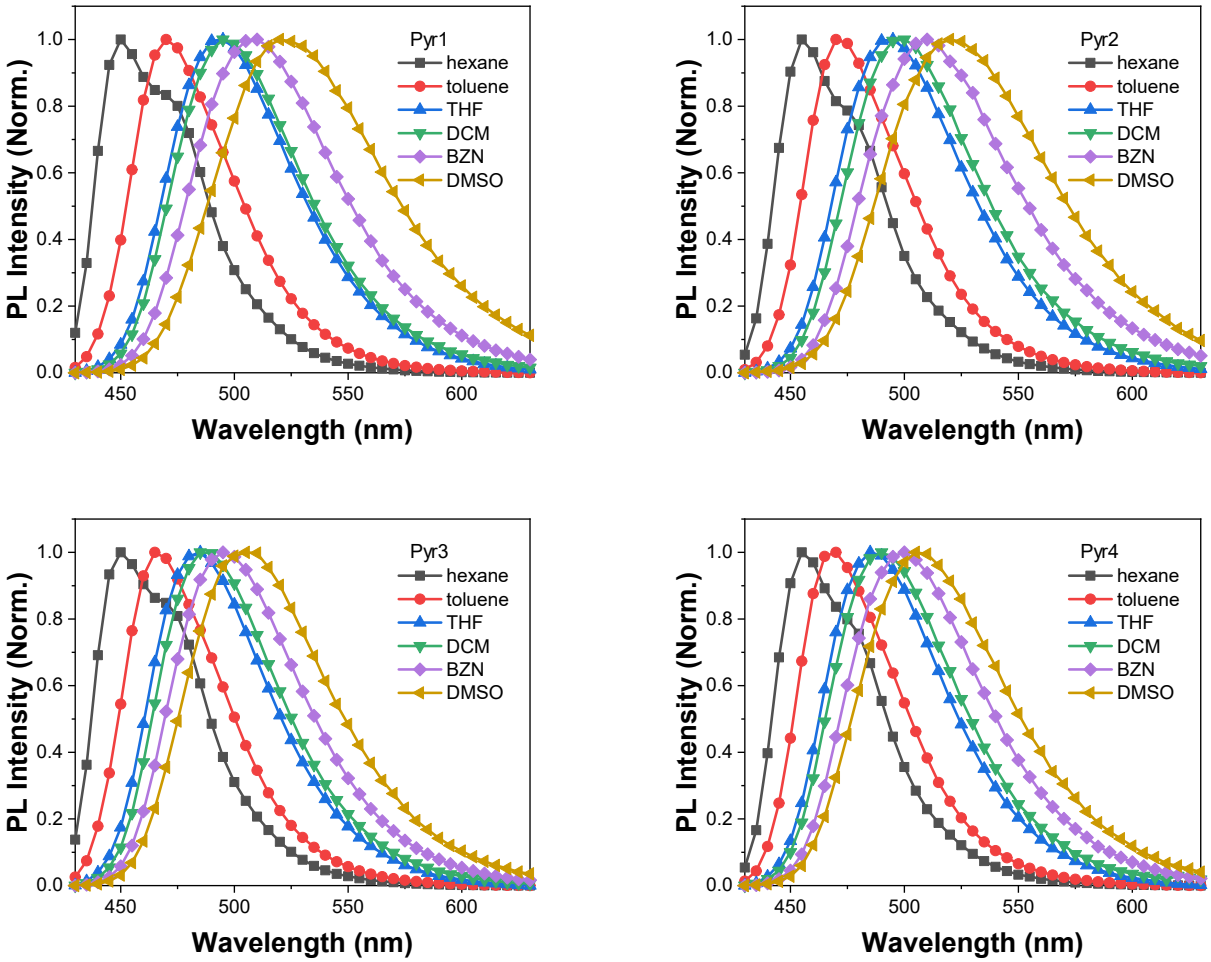

Figure S15. Time-resolved emission spectra (TRES) of the pyrene derivatives in this study in various solvents (hexane, toluene, THF, dichloromethane (DCM), benzonitrile (BZN), and DMSO). All TRES data were fit with single exponential with time constants obtained from Figure 3(c).

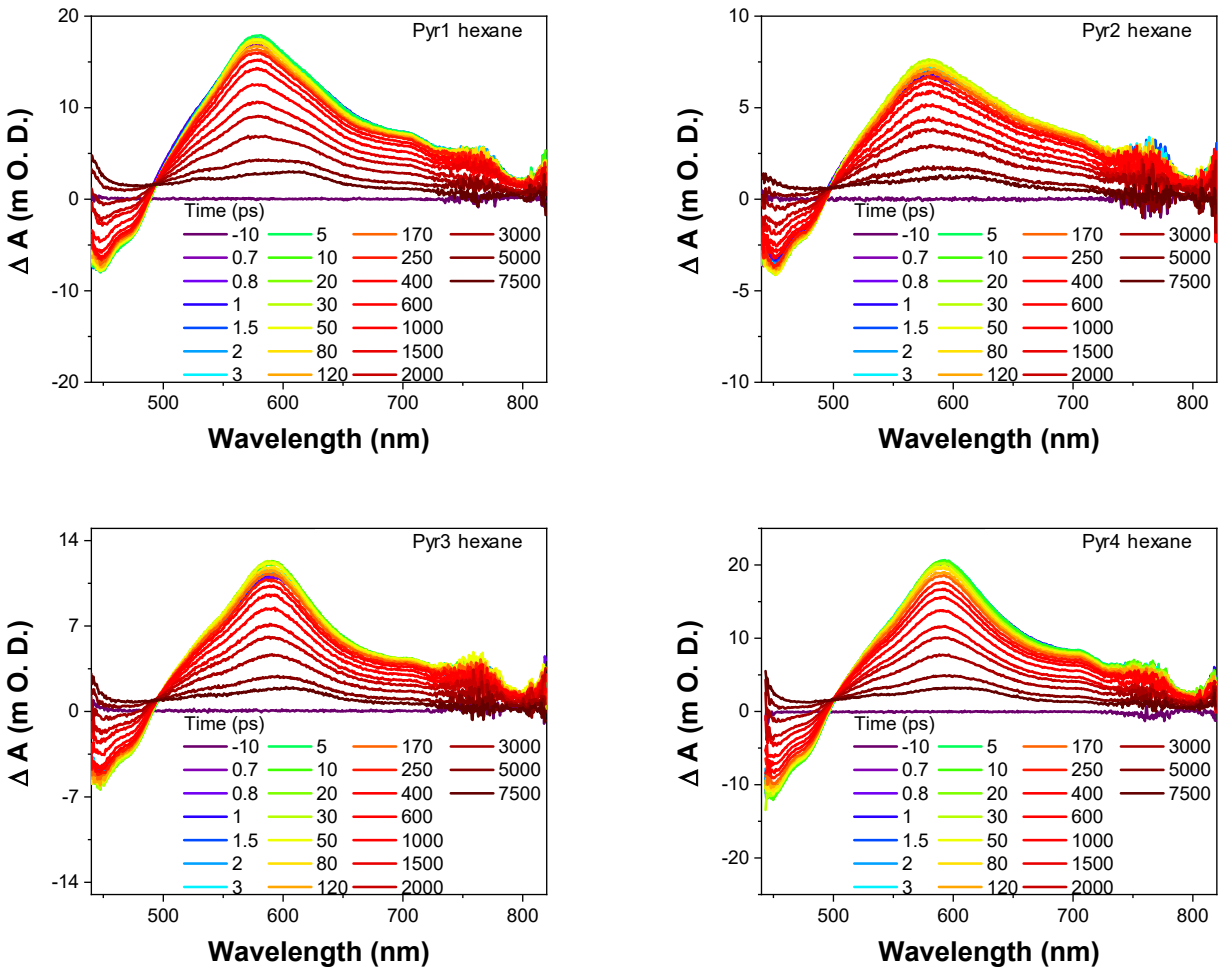

Figure S16. TA spectra of the pyrene derivatives in this study in hexane (λ_{pump} = 350 nm @ 70 μW).

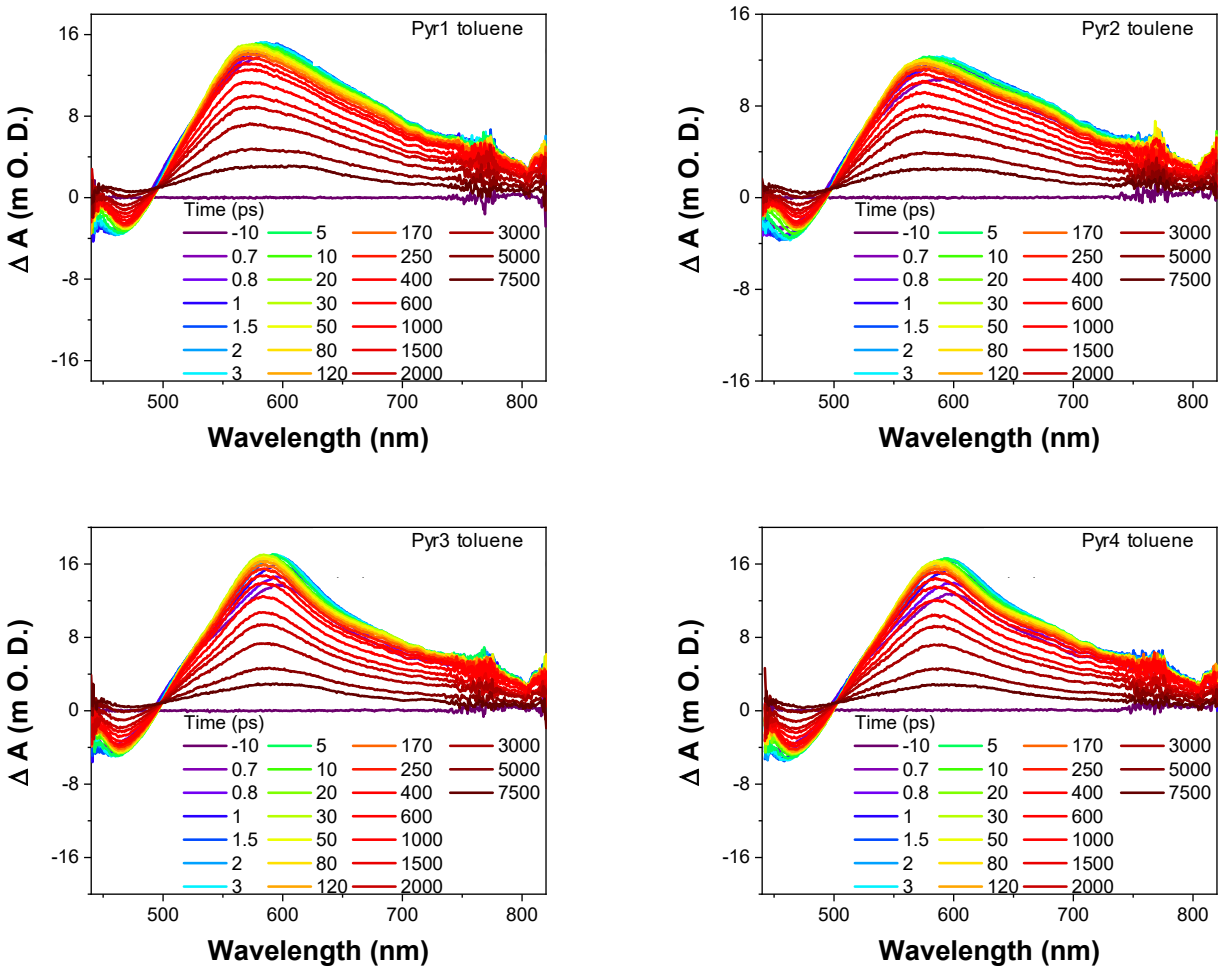

Figure S17. TA spectra of the pyrene derivatives in this study in toluene (λ_{pump} = 350 nm @ 70 μW).

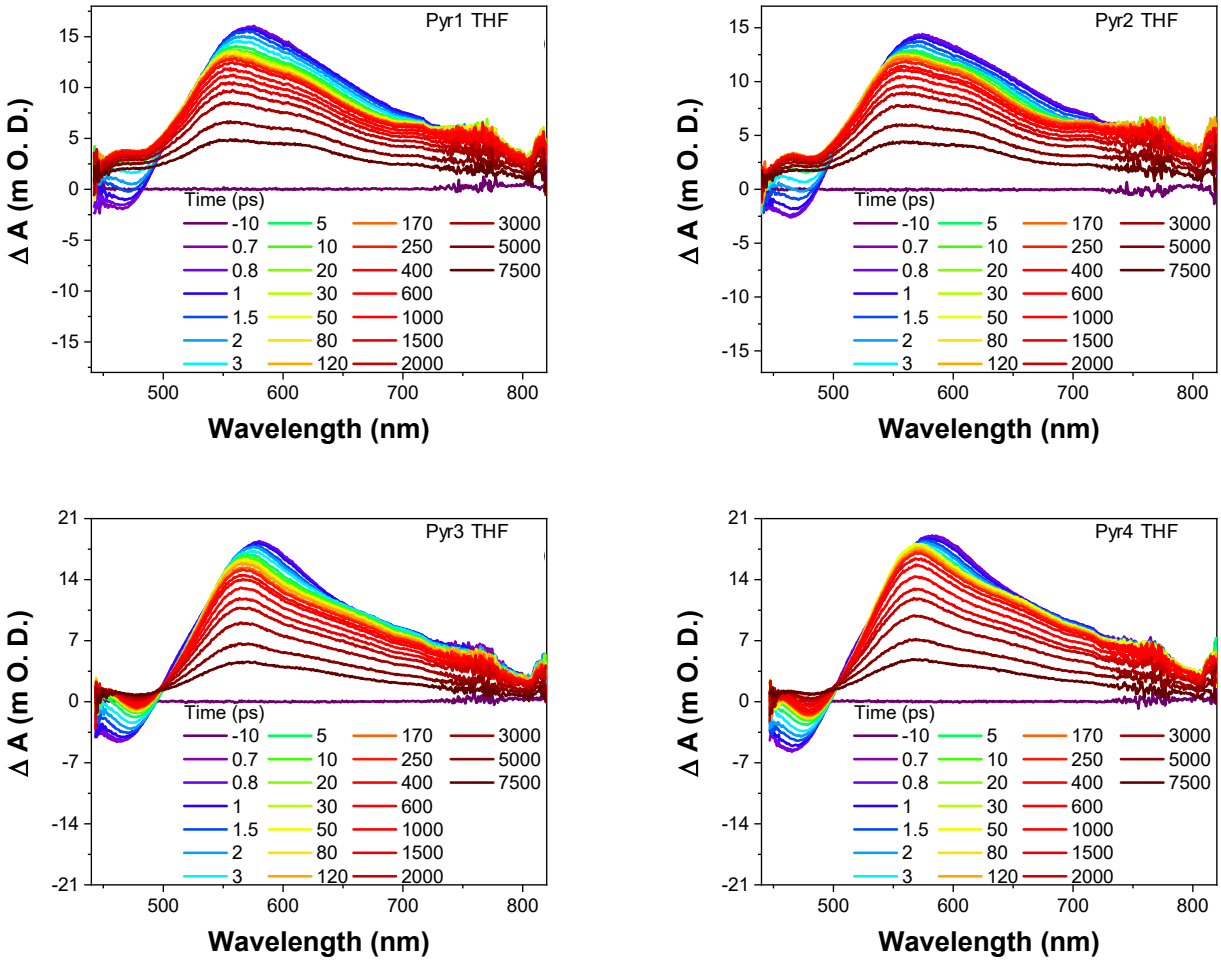

Figure S18. TA spectra of the pyrene derivatives in this study in THF (λ_{pump} = 350 nm @ 70 μW).

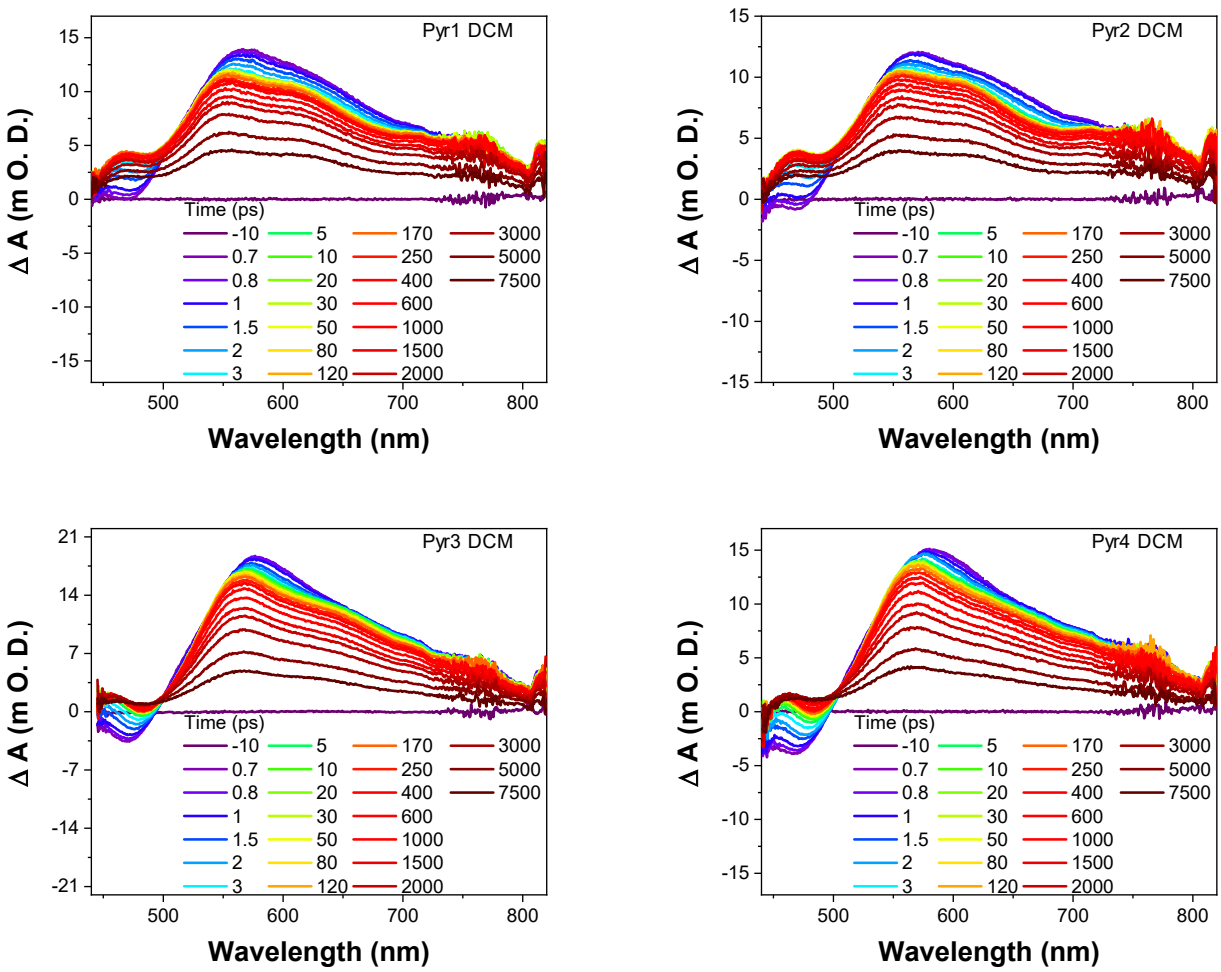

Figure S19. TA spectra of the pyrene derivatives in this study in dichloromethane (λ_{pump} = 350 nm @ 70 μW).

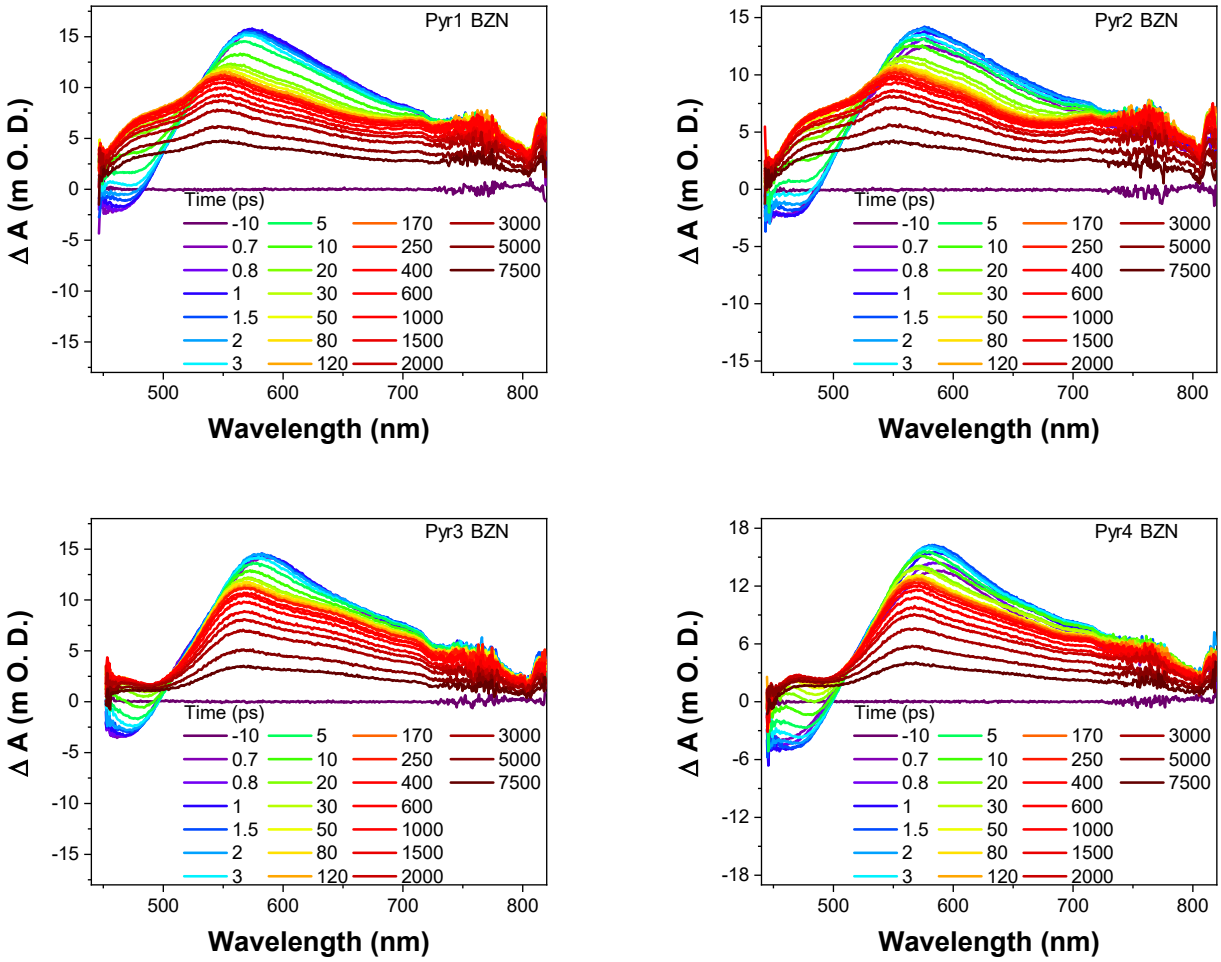

Figure S20. TA spectra of the pyrene derivatives in this study in benzonitrile (λ_{pump} = 350 nm @ 70 μW).

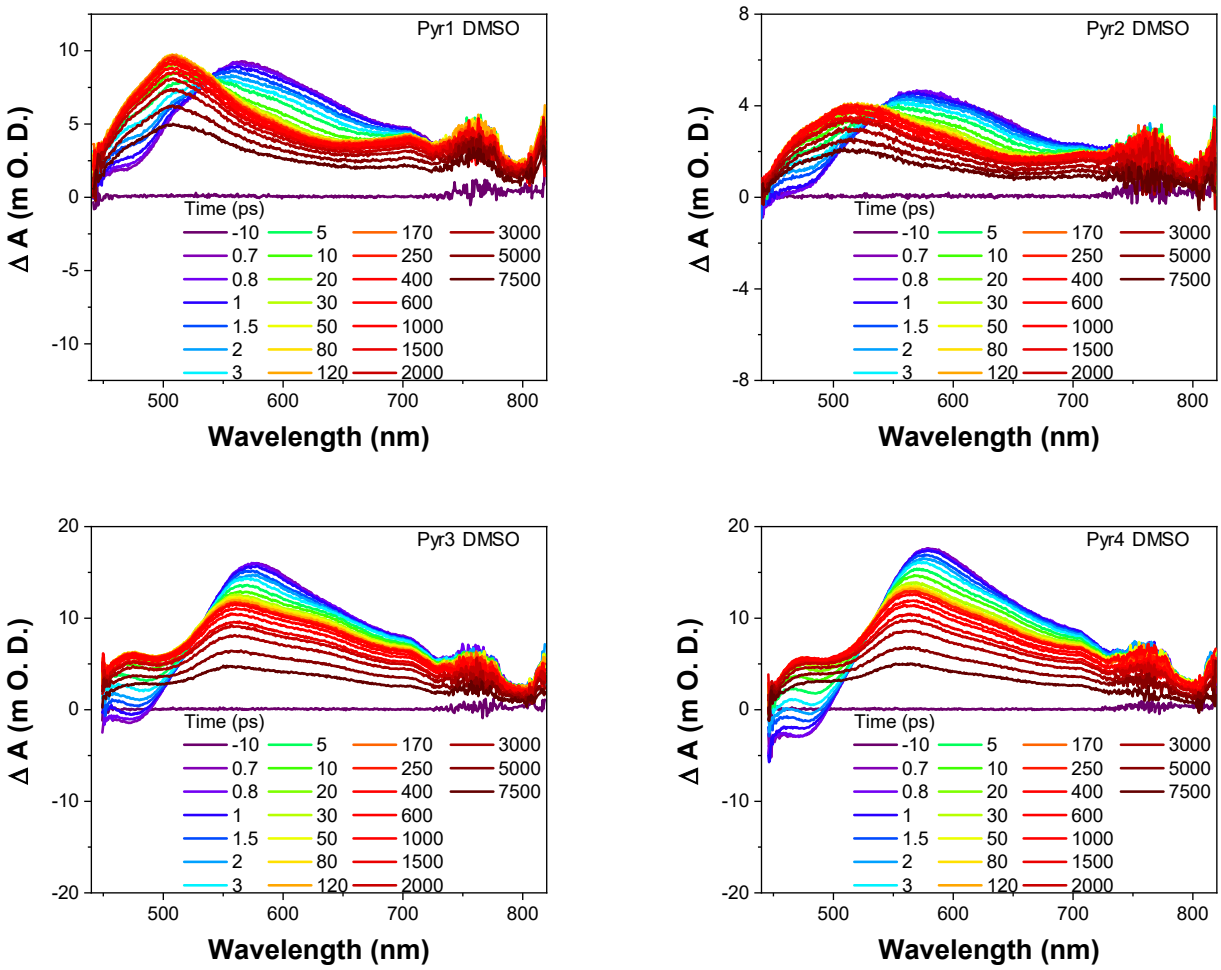

Figure S21. TA spectra of the pyrene derivatives in this study in DMSO (λ_{pump} = 350 nm @ 70 μW).

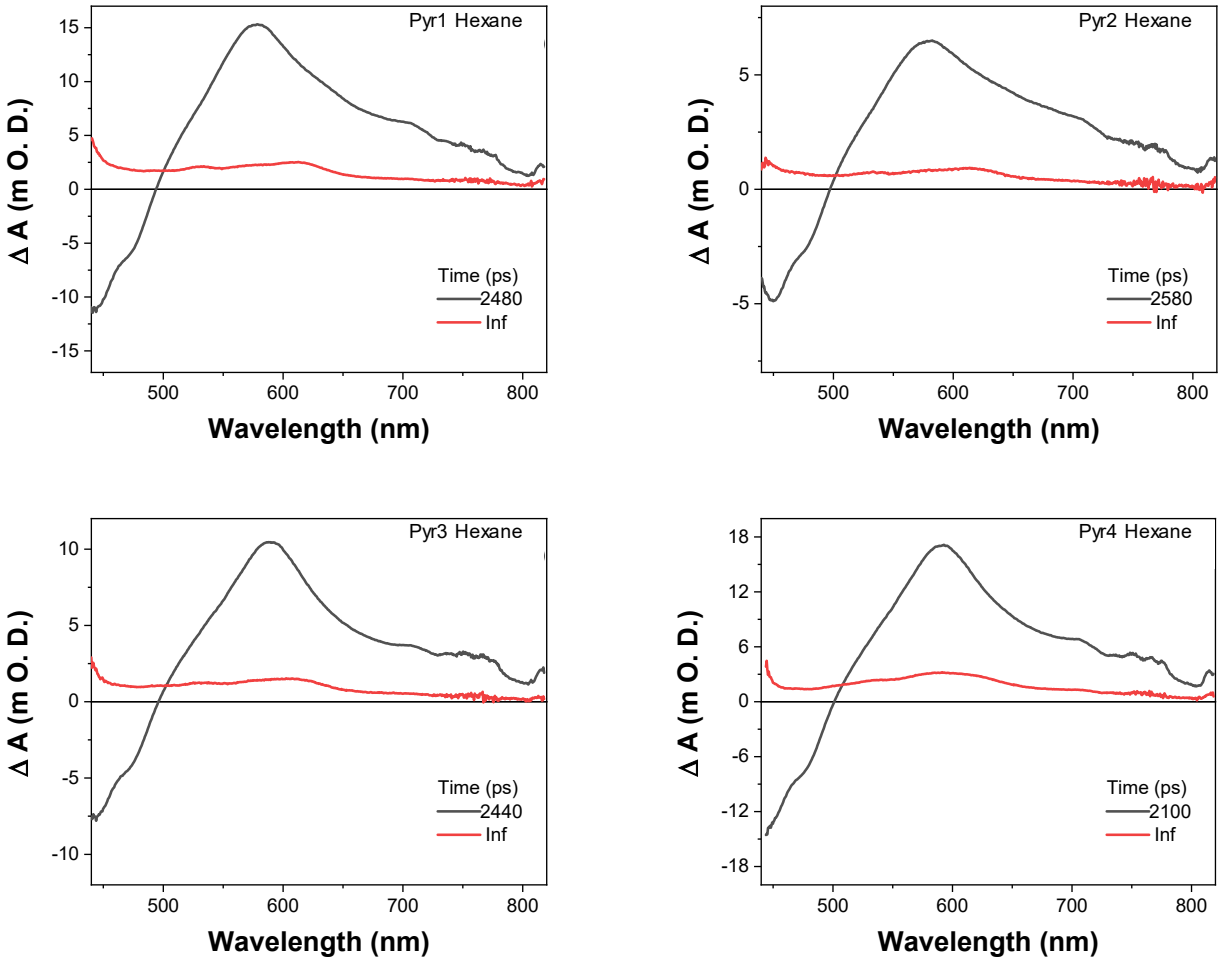

Figure S22. Decay associated spectra of the pyrene derivatives in this study in hexane (λ_{pump} = 350 nm @ 70 μW).

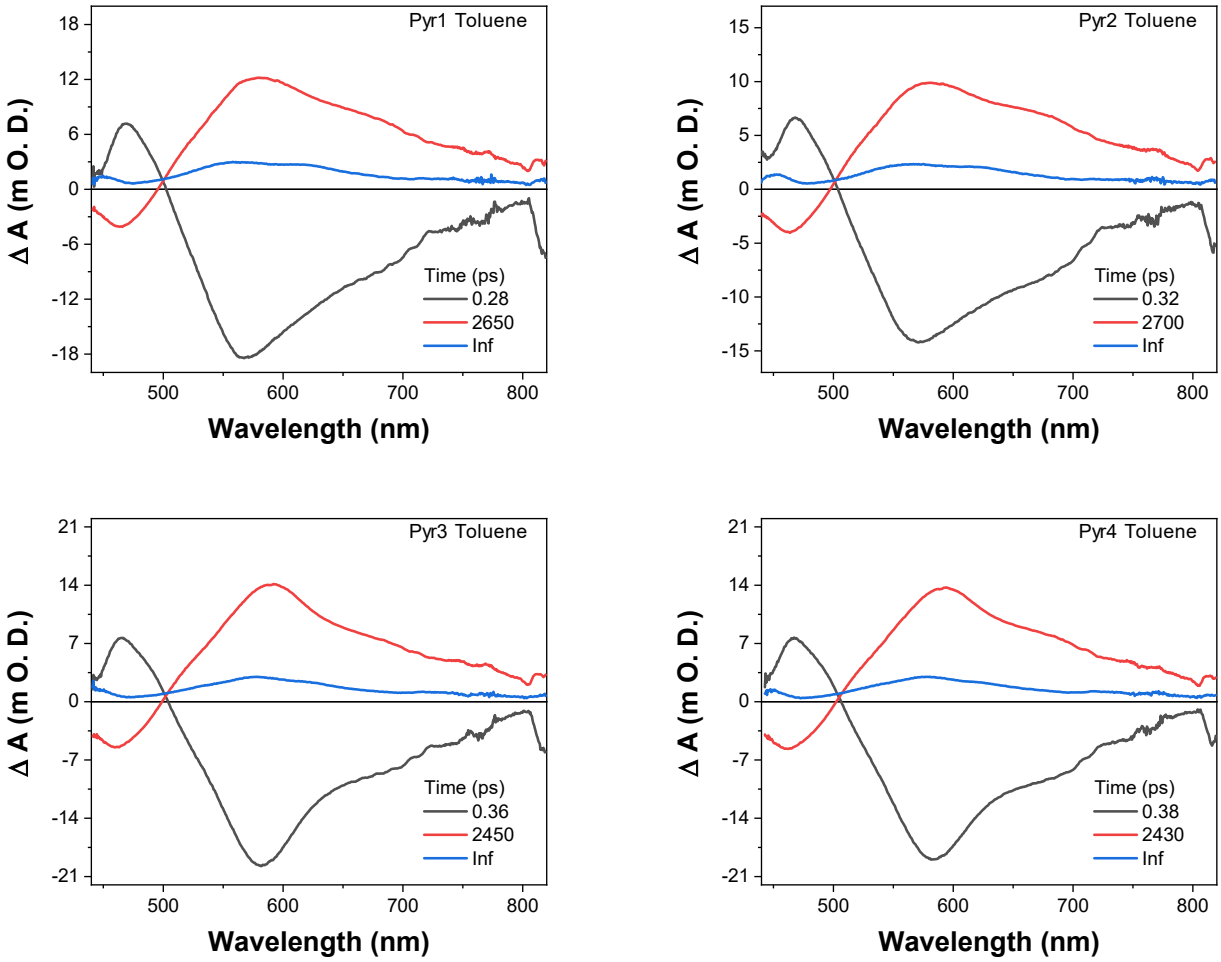

Figure S23. Decay associated spectra of the pyrene derivatives in this study in toluene (λ_{pump} = 350 nm @ 70 μW).

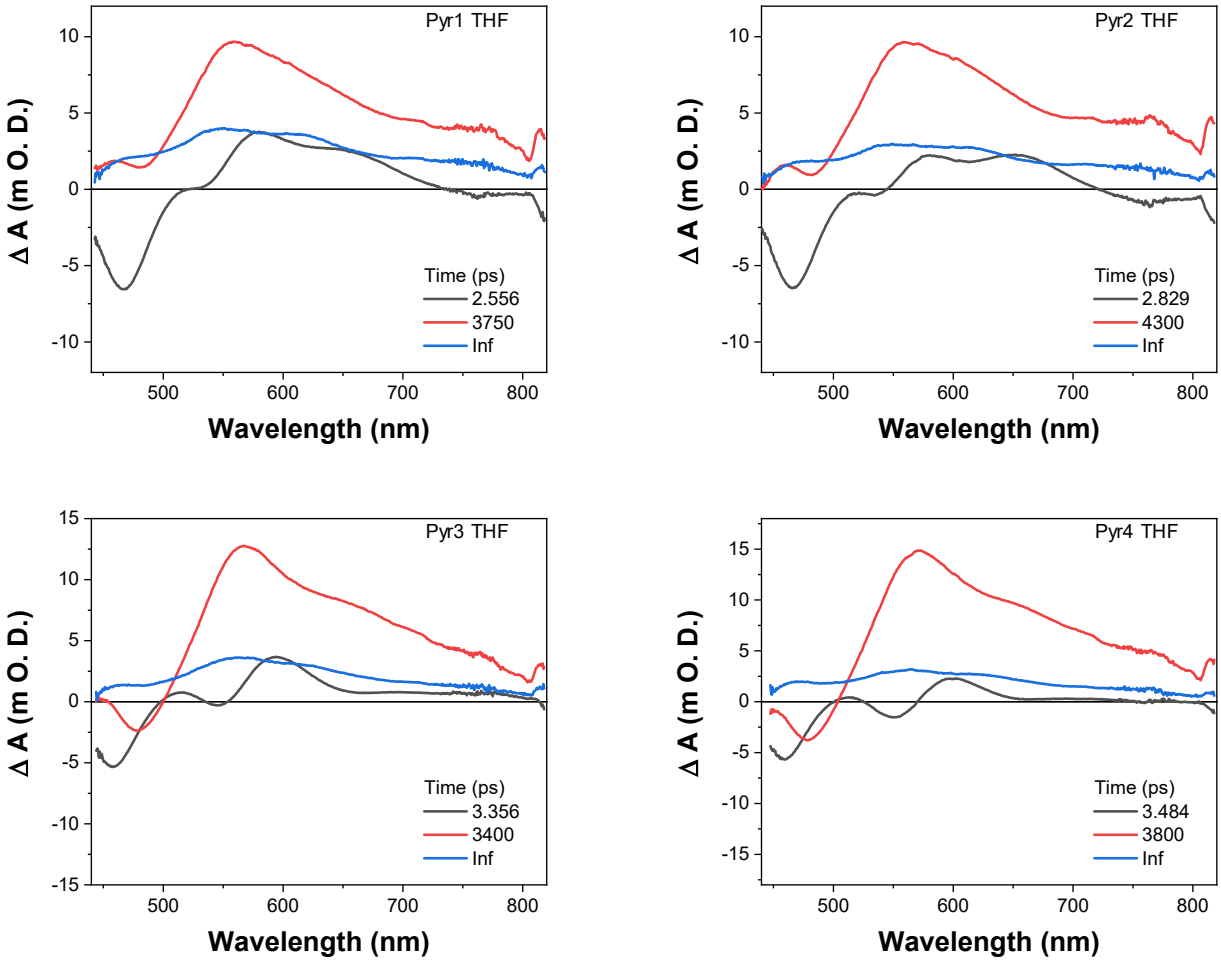

Figure S24. Decay associated spectra of the pyrene derivatives in this study in THF (λ_{pump} = 350 nm @ 70 μW).

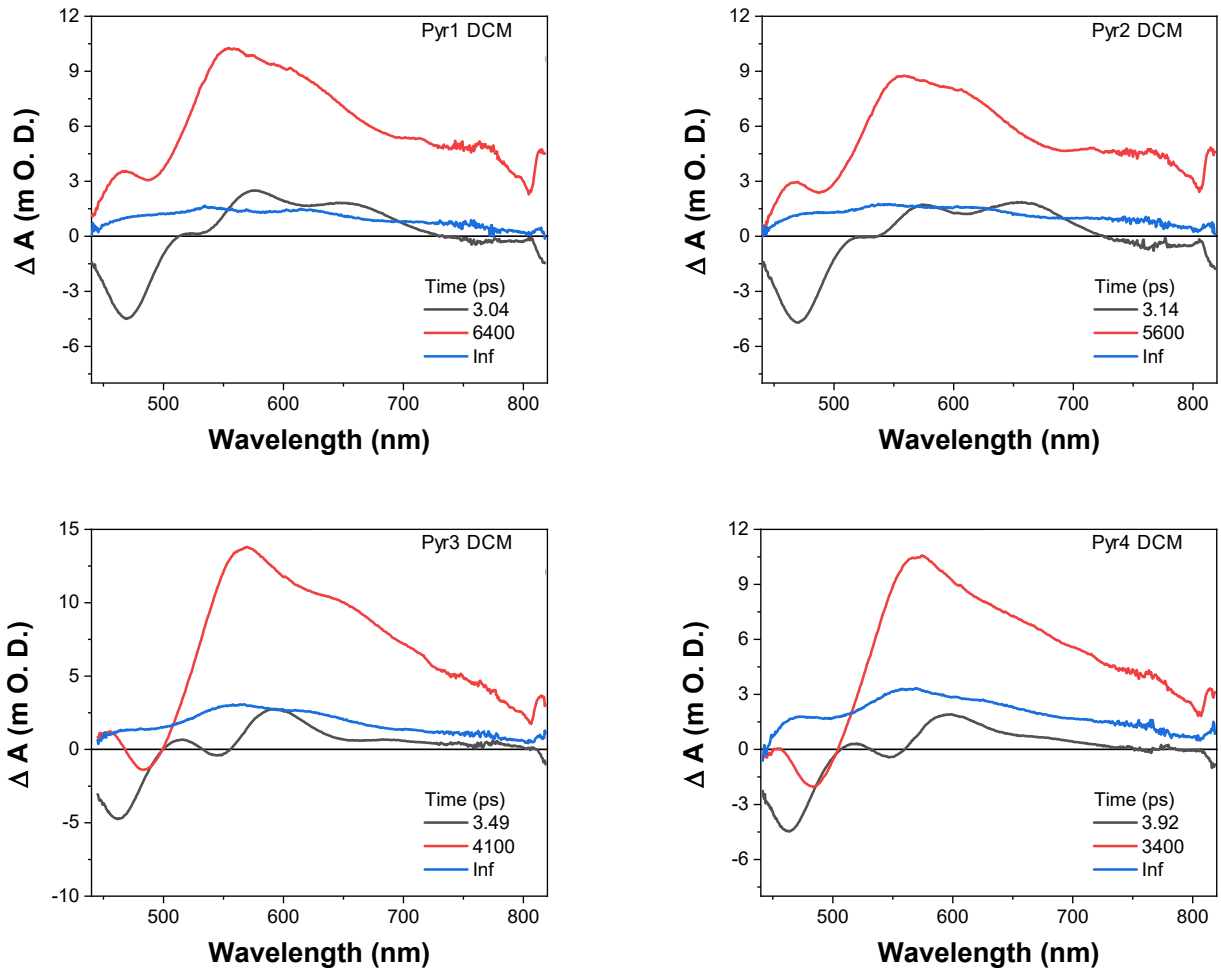

Figure S25. Decay associated spectra of the pyrene derivatives in this study in dichloromethane (λ_{pump} = 350 nm @ 70 μW).

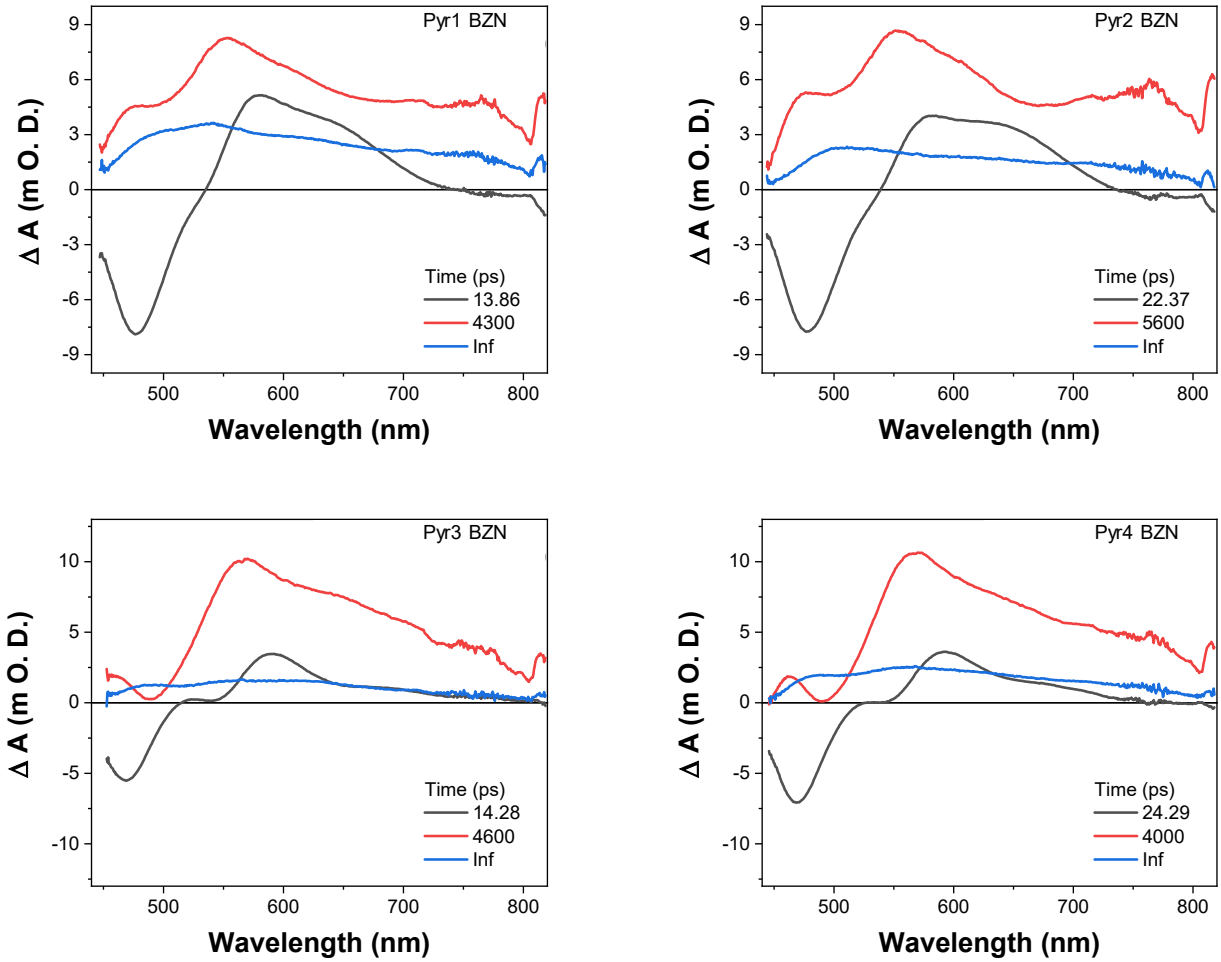

Figure S26. Decay associated spectra of the pyrene derivatives in this study in benzonitrile (λ_{pump} = 350 nm @ 70 μW).

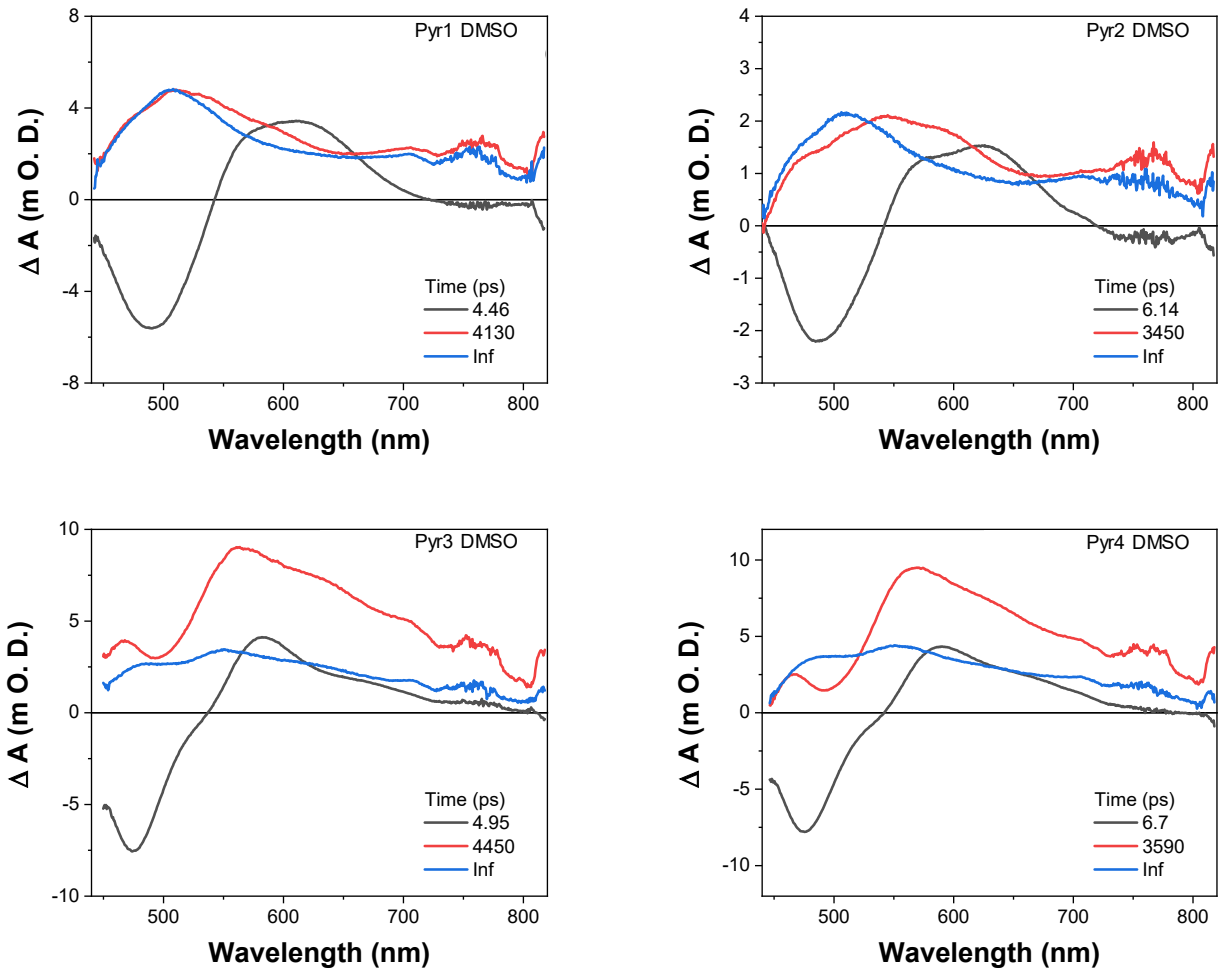

Figure S27. Decay associated spectra of the pyrene derivatives in this study in DMSO (λ_{pump} = 350 nm @ 70 μW).

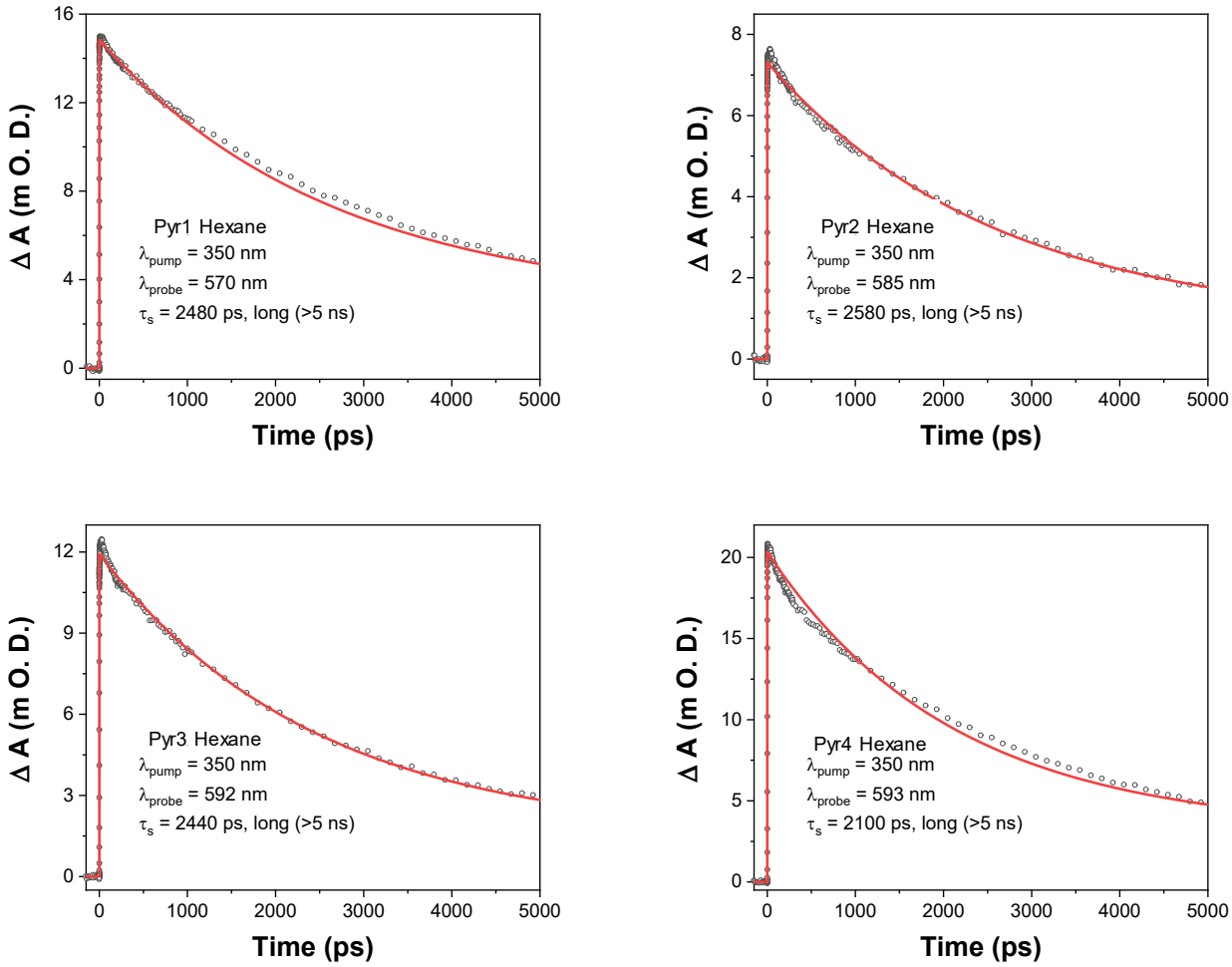

Figure S28. Decay profiles of the pyrene derivatives in this study in hexane.

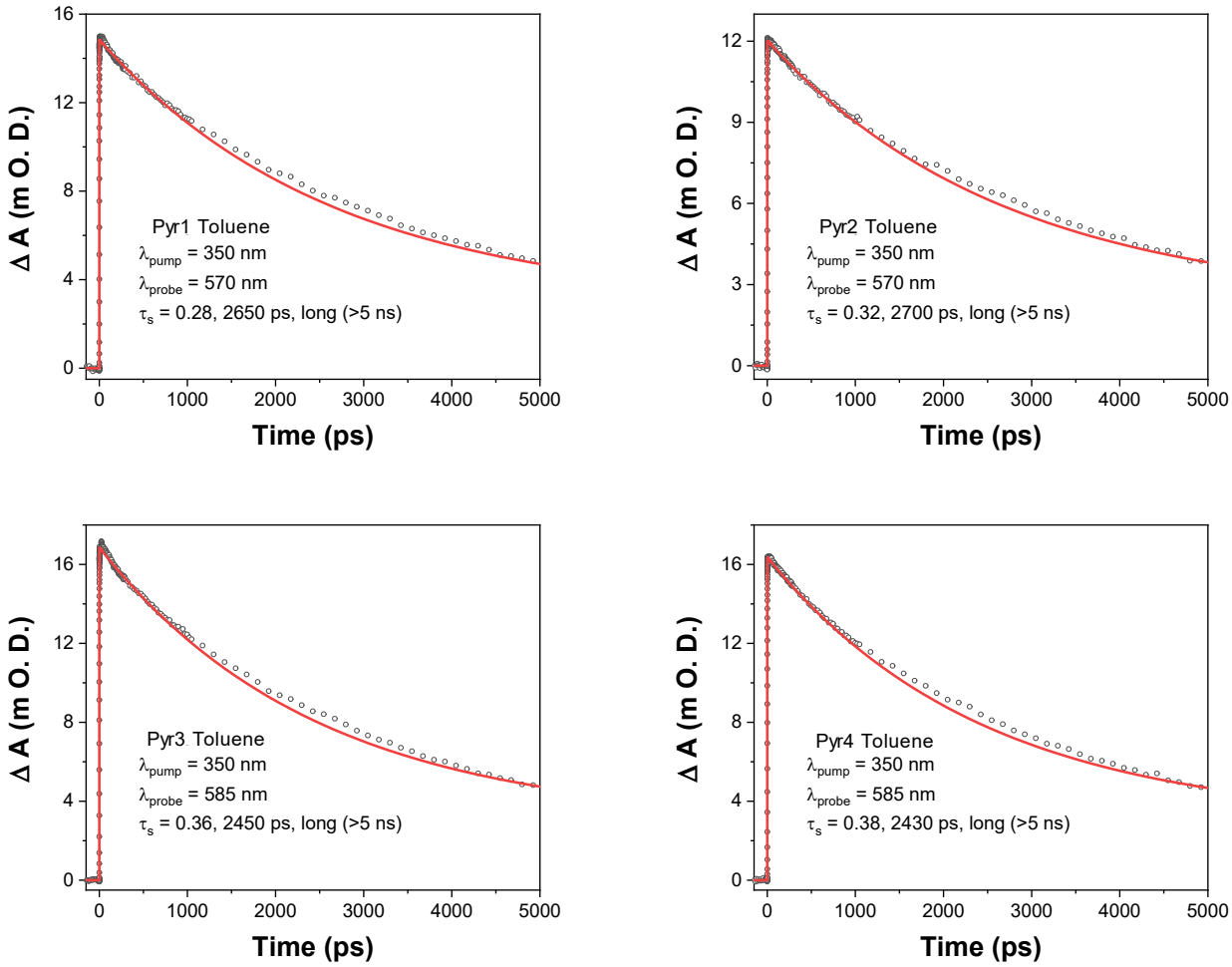

Figure S29. Decay profiles of the pyrene derivatives in this study in toluene.

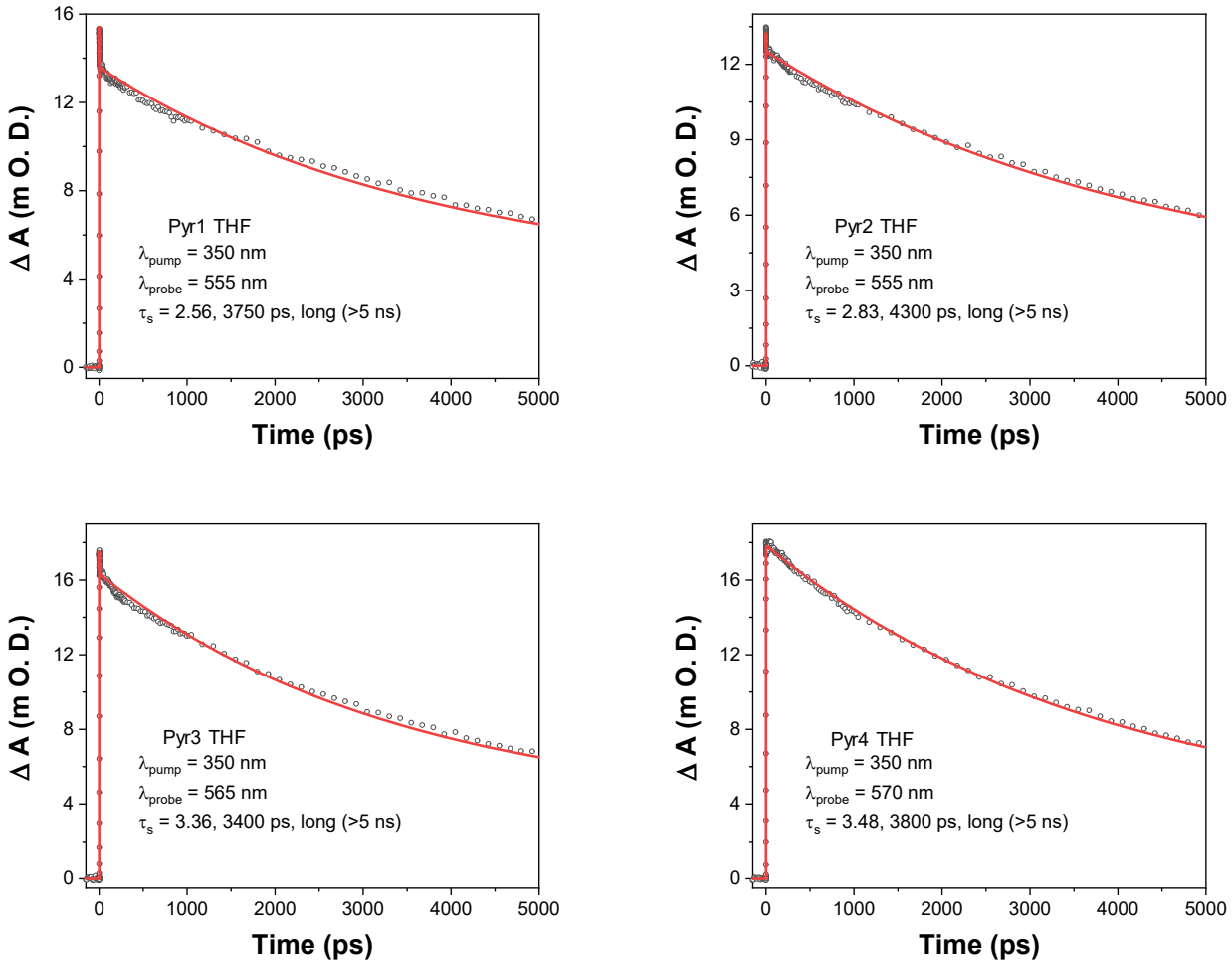

Figure S30. Decay profiles of the pyrene derivatives in this study in THF.

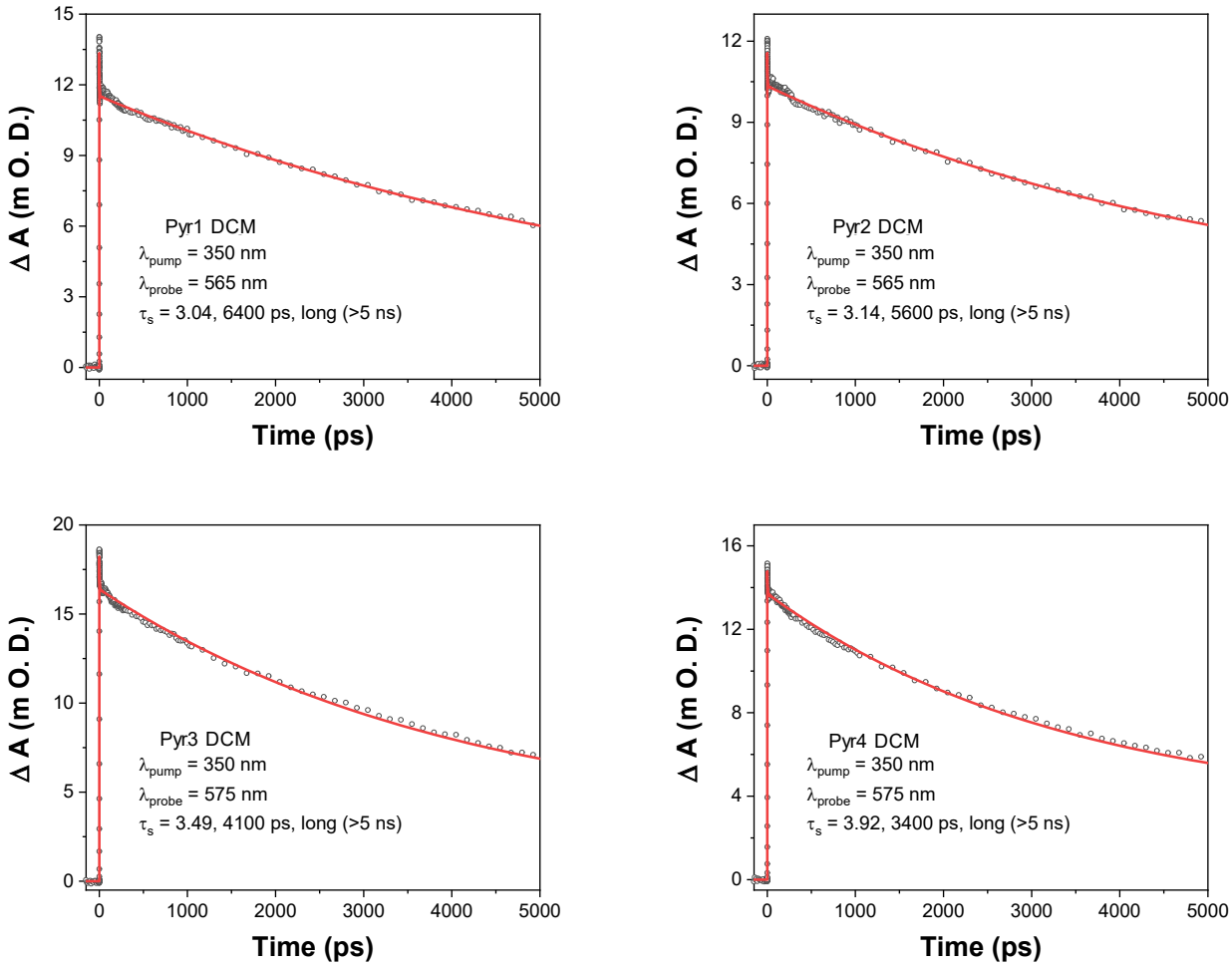

Figure S31. Decay profiles of the pyrene derivatives in this study in dichloromethane.

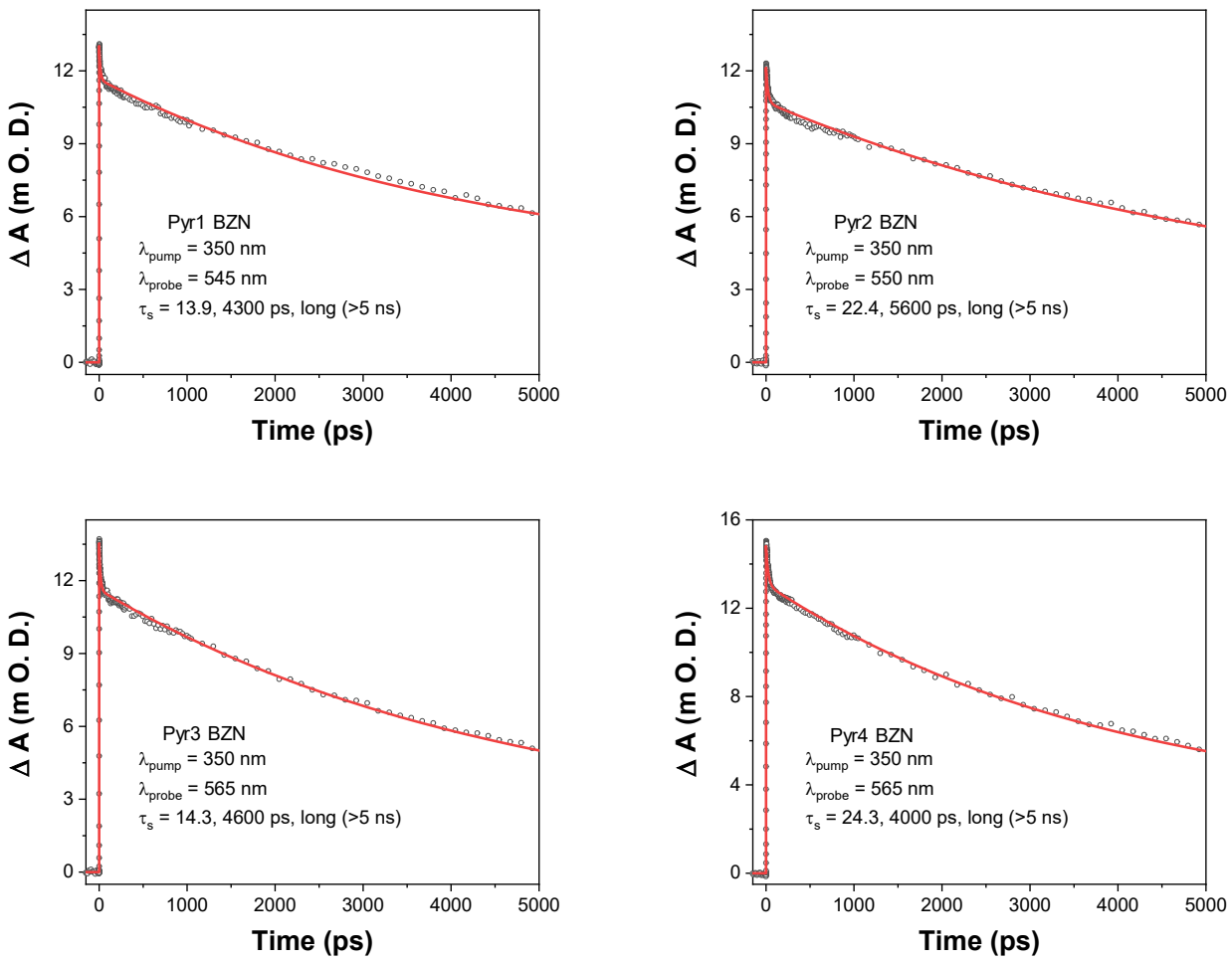

Figure S32. Decay profiles of the pyrene derivatives in this study in benzonitrile.

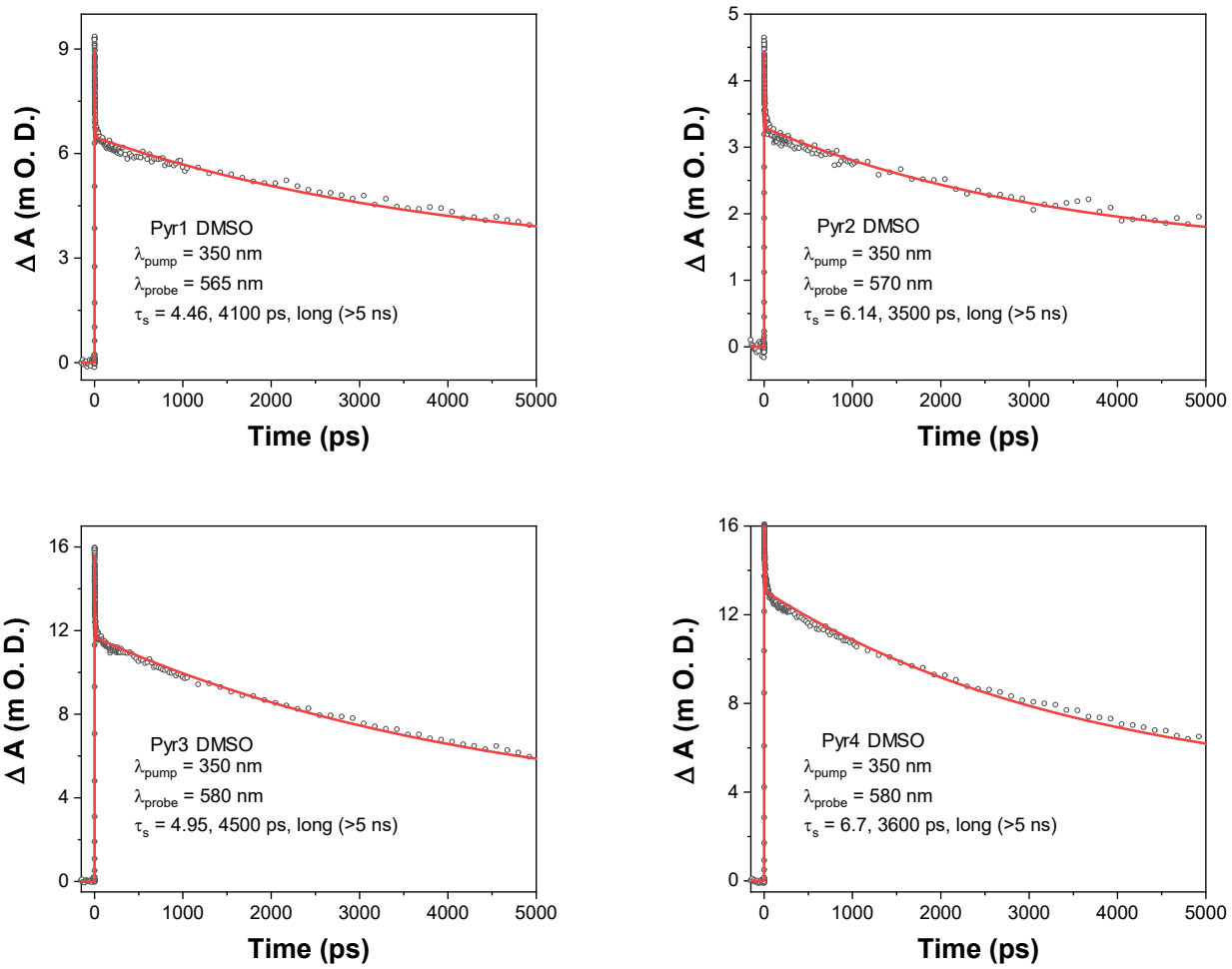

Figure S33. Decay profiles of the pyrene derivatives in this study in DMSO.

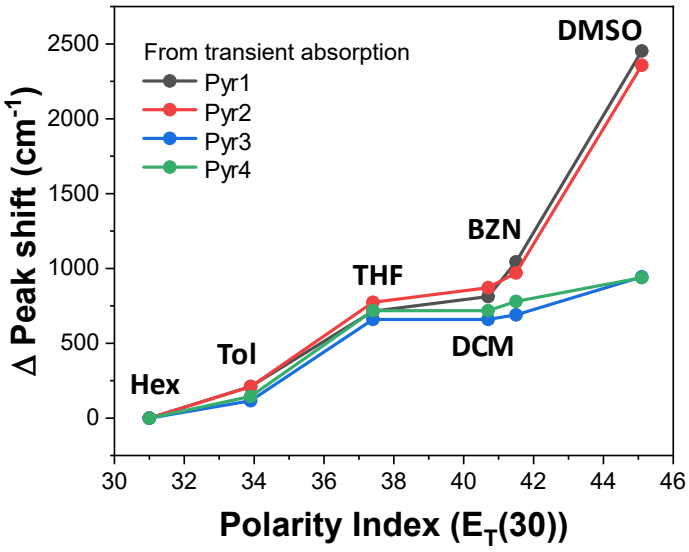

Figure S34. Differences in the positions of the peaks in the TA spectra of the initial and final states of the pyrene derivatives in this study in various solvents (hexane, toluene, THF, dichloromethane (DCM), benzonitrile (BZN), and DMSO).

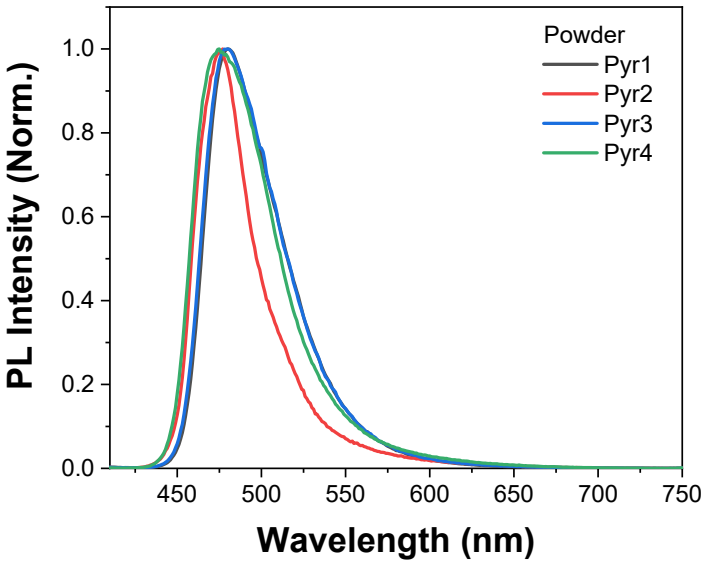

Figure S35. Fluorescence spectra of pyrene derivatives in the solid state

Table S1. The photophysical properties of the pyrene derivatives based on the results in Figure 1. The units of all the data in the table are nm.

Unit (nm)	Pyr1			Pyr2			Pyr3			Pyr4		
	Abs (Max)	Emi (Max)	Emi (FWHM)	Abs (Max)	Emi (Max)	Emi (FWHM)	Abs (Max)	Emi (Max)	Emi (FWHM)	Abs (Max)	Emi (Max)	Emi (FWHM)
Hexane	421	449	51	425	456	51	422	449	53	428	456	50
Toluene	420	472	53	422	473	52	422	467	53	427	470	50
THF	416	493	65	418	493	65	419	485	61	424	487	61
DCM	415	497	69	417	499	70	420	488	65	424	492	67
BZN	418	509	73	421	509	73	423	496	67	428	499	68
DMSO	415	522	89	417	522	87	420	506	77	425	508	80

Table S2. The Stokes shift, fluorescence quantum yield and lifetime of the pyrene derivatives.

	Pyr1			Pyr2			Pyr3			Pyr4		
	Stokes shift (cm^{-1})	Φ_{fl}	τ_{fl} (ns)	Stokes shift (cm^{-1})	Φ_{fl}	τ_{fl} (ns)	Stokes shift (cm^{-1})	Φ_{fl}	τ_{fl} (ns)	Stokes shift (cm^{-1})	Φ_{fl}	τ_{fl} (ns)
Hexane	1481	0.562	2.69	1600	0.605	2.93	1425	0.625	2.79	1435	0.631	2.95
Toluene	2623	0.723	3.79	2555	0.747	3.94	2283	0.765	3.45	2143	0.782	3.56
THF	3754	0.795	7.15	3639	0.8	7.34	3248	0.836	5.7	3051	0.87	6.14
DCM	3976	0.911	7.4	3941	0.915	7.46	3318	0.915	5.92	3260	0.919	6.23
BZN	4277	0.93	8.27	4107	0.942	8.28	3479	0.944	6.2	3324	0.957	6.5
DMSO	4939	0.851	10.84	4824	0.999	10.09	4047	0.999	7.82	3844	0.999	8.23

Table S3 The radiative and non-radiative rates of the pyrene derivatives. The units of all the data in the table are 10^{-9} s^{-1}.

Unit (10^{-9} s^{-1})	Pyr1		Pyr2		Pyr3		Pyr4	
	k_r	k_{nr}	k_r	k_{nr}	k_r	k_{nr}	k_r	k_{nr}
Hexane	0.209	0.163	0.206	0.135	0.224	0.134	0.214	0.125
Toluene	0.191	0.073	0.190	0.064	0.222	0.068	0.220	0.061
THF	0.111	0.029	0.109	0.027	0.147	0.029	0.142	0.021
DCM	0.123	0.012	0.123	0.011	0.155	0.014	0.148	0.013
BZN	0.112	0.0085	0.114	0.007	0.152	0.009	0.147	0.0066
DMSO	0.079	0.013	0.099	0.00099	0.128	0.0013	0.121	0.0012

Table S4. The TA decay components of the pyrene derivatives. The time constants are obtained by fitting the results in Figures S27-S32 with bi-/tri-exponential function having two/three decay components.

	Pyr1	Pyr2	Pyr3	Pyr4
Hexane	2480 ps, > 5 ns	2580 ps, > 5 ns	2440 ps, > 5 ns	2100 ps, > 5 ns
Toluene	0.28 ps, 2650 ps, > 5 ns	0.32 ps, 2700 ps, > 5 ns	0.36 ps, 2450 ps, > 5 ns	0.38 ps, 2430 ps, > 5 ns
THF	2.56 ps, 3750 ps, > 5 ns	2.83 ps, 4300 ps, > 5 ns	3.36 ps, 3400 ps, > 5 ns	3.48 ps, 3800 ps, > 5 ns
DCM	3.04 ps, 6400 ps, > 5 ns	3.14 ps, 5600 ps, > 5 ns	3.49 ps, 4100 ps, > 5 ns	3.92 ps, 3400 ps, > 5 ns
BZN	13.9 ps, 4300 ps, > 5 ns	22.4 ps, 5600 ps, > 5 ns	14.3 ps, 4600 ps, > 5 ns	24.3 ps, 4000 ps, > 5 ns
DMSO	4.46 ps, 4100 ps, > 5 ns	6.14 ps, 3500 ps, > 5 ns	4.95 ps, 4500 ps, > 5 ns	6.7 ps, 3600 ps, > 5 ns